

University of Kentucky

UKnowledge

---

Theses and Dissertations--Earth and  
Environmental Sciences

Earth and Environmental Sciences

---


2023

## FIELD TESTS OF A UAV-COMPATIBLE SPECTROMETER TO EVALUATE ITS SUITABILITY FOR DETAILED SOIL RADON POTENTIAL MAPPING

Alexandria Briahnne Thomas

University of Kentucky, [applerocks0402@gmail.com](mailto:applerocks0402@gmail.com)

Author ORCID Identifier:

 <https://orcid.org/0009-0004-9395-2445>

Digital Object Identifier: <https://doi.org/10.13023/etd.2023.293>

[Right click to open a feedback form in a new tab to let us know how this document benefits you.](#)

### Recommended Citation

Thomas, Alexandria Briahnne, "FIELD TESTS OF A UAV-COMPATIBLE SPECTROMETER TO EVALUATE ITS SUITABILITY FOR DETAILED SOIL RADON POTENTIAL MAPPING" (2023). *Theses and Dissertations--Earth and Environmental Sciences*. 100.

[https://uknowledge.uky.edu/ees\\_etds/100](https://uknowledge.uky.edu/ees_etds/100)

This Master's Thesis is brought to you for free and open access by the Earth and Environmental Sciences at UKnowledge. It has been accepted for inclusion in Theses and Dissertations--Earth and Environmental Sciences by an authorized administrator of UKnowledge. For more information, please contact [UKnowledge@lsv.uky.edu](mailto:UKnowledge@lsv.uky.edu).

## **STUDENT AGREEMENT:**

I represent that my thesis or dissertation and abstract are my original work. Proper attribution has been given to all outside sources. I understand that I am solely responsible for obtaining any needed copyright permissions. I have obtained needed written permission statement(s) from the owner(s) of each third-party copyrighted matter to be included in my work, allowing electronic distribution (if such use is not permitted by the fair use doctrine) which will be submitted to UKnowledge as Additional File.

I hereby grant to The University of Kentucky and its agents the irrevocable, non-exclusive, and royalty-free license to archive and make accessible my work in whole or in part in all forms of media, now or hereafter known. I agree that the document mentioned above may be made available immediately for worldwide access unless an embargo applies.

I retain all other ownership rights to the copyright of my work. I also retain the right to use in future works (such as articles or books) all or part of my work. I understand that I am free to register the copyright to my work.

## **REVIEW, APPROVAL AND ACCEPTANCE**

The document mentioned above has been reviewed and accepted by the student's advisor, on behalf of the advisory committee, and by the Director of Graduate Studies (DGS), on behalf of the program; we verify that this is the final, approved version of the student's thesis including all changes required by the advisory committee. The undersigned agree to abide by the statements above.

Alexandria Briahnne Thomas, Student

William C. Haneberg, Major Professor

Michael M. McGlue, Director of Graduate Studies

FIELD TESTS OF A UAV-COMPATIBLE SPECTROMETER TO EVALUATE ITS  
SUITABILITY FOR DETAILED SOIL RADON POTENTIAL MAPPING

---

THESIS

---

A thesis submitted in partial fulfillment of the  
requirements for the degree of Master of Science in the  
College of Arts and Sciences  
at the University of Kentucky

By

Alexandria Briahnne Thomas

Lexington, Kentucky

Director: Dr. William C. Haneberg, Professor of Earth and Environmental Sciences

Lexington, Kentucky

2023

Copyright © Alexandria Briahnne Thomas 2023  
<https://orcid.org/0009-0004-9395-2445>

## ABSTRACT OF THESIS

### FIELD TESTS OF A UAV-COMPATIBLE SPECTROMETER TO EVALUATE ITS SUITABILITY FOR DETAILED SOIL RADON POTENTIAL MAPPING

As part of ongoing research on radionuclide mapping and radon hazard characterization, field tests were performed to evaluate the suitability and limitations of a UAV-compatible gamma spectrometer. To date, this data set includes completed stationary data collection, mobile ground collection, multi-level UAV flights over a known material transition, as well as redundant ground and multi-level UAV data collection over a relatively uniform area. Total counts were used as a measure of soil radionuclide levels for our data collected above background. Although our test sites were in regions underlain by bedrock with high indoor radon levels, uranium counts were barely above background levels. The spectrometer can delineate obvious surface material contrasts (e.g., grass versus asphalt or concrete) analogous to boundaries such as faults juxtaposing different rock units. As the height of the instrument increases above a single surface type, the sensitivity of the spectrometer decreases linearly above the ground while the on-ground footprint increases geometrically. This limits the ability to resolve geologic boundaries. In areas covered by distinctly different surface types, the variation in counts is a function of both altitude and the proportion of each surface type within the footprint of the spectrometer at that location and height. In some cases, height appears to contribute to an increase in counts if the instrument is over a low-count surface material, but the complete spectrometer footprint is dominated by a high-count surface material. Ongoing research will quantify background variability to help identify local variations in a low signal-to-noise (low gamma) environment, including the feasibility of stacking results from multiple single-height flights or profiles to cancel noise and amplify changes across geologic boundaries. Results from multi-level flights will also contribute to our understanding of instrument sensitivity and spatial resolution as functions of flying height.

KEYWORDS: UAV, spectrometer, background, surface type, photon, total count

---

Alexandria Briahnnne Thomas

*(Name of Student)*

---

04/27/2023

Date

FIELD TESTS OF A UAV-COMPATIBLE SPECTROMETER TO EVALUATE ITS  
SUITABILITY FOR DETAILED SOIL RADON POTENTIAL MAPPING

By

Alexandria Briahnne Thomas

William C. Haneberg

---

Director of Thesis

Michael M. McGlue

---

Director of Graduate Studies

04/27/2023

---

Date

## DEDICATION

To my mother, my biggest cheerleader.  
Love and light.

## ACKNOWLEDGMENTS

First, my Thesis Chair, William C. Haneberg, exemplifies the high-quality scholarship to which I aspire. Next, I wish to thank the complete Thesis Committee, respectively: Dr. William “Drew” Andrews, Dr. Matt Crawford, and Dr. Andrea Erhardt. Each individual provided insights that guided and challenged my thinking, substantially improving the finished product.

This research was made possible by Grant P30 ES026529 from the National Institute of Environmental Health Sciences. Its contents are solely the responsibility of the authors and do not necessarily represent the official views of the NIEHS. A special thank you to the Kentucky Geological Survey which funded my research position and the Earth and Environmental Science Department of the College of Arts and Sciences for guiding me through my Master of Science in Geological Sciences program.

In addition to the technical and instrumental assistance above, I received equally important assistance from family and friends. My father, sister, and boyfriend provided ongoing support throughout the thesis process and technical assistance critical for completing the project in a timely manner.

## TABLE OF CONTENTS

ACKNOWLEDGMENTS .....	iv
LIST OF TABLES .....	vii
LIST OF FIGURES .....	viii
CHAPTER 1. Introduction.....	1
1.1 Introduction.....	1
1.1 Kentucky Geology and Indoor-Radon Potential .....	6
1.2 Previous Works.....	8
CHAPTER 2. Background .....	11
2.1 Radon Geochemistry.....	11
2.2 Study Area .....	15
2.3 Spectrometer and UAV.....	19
2.3.1 Instrumentation.....	22
CHAPTER 3. Methods.....	25
3.1 Overview .....	25
CHAPTER 4. Results.....	31
4.1 Results.....	31
4.1.1 GPS Reliability – Stationary Test .....	31
4.1.2 Spectrometer Variability – Stationary Test.....	34
4.1.3 Effects of Environment and Background .....	36
4.1.4 Duration Variability – Stationary Test .....	38
4.1.5 Effect of Height Above the Ground – Vertical Test.....	40
4.1.6 Replicability .....	42
4.1.7 Recognizing Different Materials.....	43
4.1.8 Footprint.....	47
4.1.9 Topographic Effect of a Sinkhole .....	49
4.1.10 Fault Transect.....	52
CHAPTER 5. Discussion .....	56
CHAPTER 6. Conclusion .....	62
APPENDICES.....	64
APPENDIX 1. PRODUCE A HISTOGRAM.....	65
APPENDIX 2. PRODUCE A STATISTICAL ANALYSIS .....	66
APPENDIX 3. PRODUCE A SCATTERPLOT AND LOGARITHMIC REGRESSION LINE .....	67



<i>APPENDIX 4. ARCGIS PRO WORKFLOW</i> .....	68
REFERENCES.....	69
VITA	77

## LIST OF TABLES

Table 3.1 Methods.....	30
Table 4.1 GPS Reliability.....	32
Table 4.2 Spectrometer Variability.....	35
Table 4.2 Continued.....	36
Table 4.3 Effect of Environment and Background.....	37
Table 4.4 Duration Variability.....	40
Table 4.5 Vertical Tests.....	42
Table 4.6 Replicability.....	43
Table 4.7 Recognizing Different Materials.....	46
Table 4.8 Footprint.....	48
Table 4.8 Continued.....	49
Table 4.9 Sinkhole.....	52
Table 4.10 Fault Transect.....	55

## LIST OF FIGURES

Figure 1.1 Indoor Radon Potential Map.....	3
Figure 1.2 Geographical Regions Map.....	5
Figure 1.3 Geological Map.....	8
Figure 2.1 Uranium Decay Series.....	12
Figure 2.2 Permeability Sketch.....	14
Figure 2.3 Inner Bluegrass and Interior Mississippian Plateau.....	16
Figure 2.4 DJI Matrice 600 Pro.....	22
Figure 2.5 GEORADiS® D230A.....	24
Figure 3.1 UgsCS by SPH Engineering.....	26
Figure 3.2 Fault Map.....	29
Figure 4.1 2D Berea Road Soccer Complex Map.....	33
Figure 4.2 Groups 19 and 24 Histograms.....	34
Figure 4.3 Groups 15, 16, and 17 Histograms.....	37
Figure 4.4 Group 34 Soil Histogram.....	39
Figure 4.5 Group 35 Asphalt Histogram.....	39
Figure 4.6 3D map of Vertical Flight Tests.....	41
Figure 4.7 Scatterplots of Vertical Height.....	41
Figure 4.8 Groups 22and 23 Histograms.....	43
Figure 4.9 Group 8 Asphalt Histogram.....	45
Figure 4.10 Group 8 Soil Histogram.....	45
Figure 4.11 Footprint Diagram.....	48
Figure 4.12 Sinkhole Contour Map.....	50
Figure 4.13 Sinkhole Lidar Map.....	51
Figure 4.14 Average Distance vs. Average Total Count Plot (Sinkhole).....	52
Figure 4.15 Moving Mean and Standard Deviation Plot.....	54

## CHAPTER 1. INTRODUCTION

### 1.1 Introduction

Radon – a dense, naturally occurring, and radioactive airborne gas formed by the alpha decay of radium – is the second leading cause of lung cancer in the United States, surpassed only by tobacco use and exposure to tobacco smoke. Approximately 21, 000 people in the United States die each year from exposure to high levels of indoor radon (*American Cancer Society, 2022; Environmental Protection Agency, 2023*). Lung cancer mortality rates have decreased as public health campaigns have encouraged tobacco reduction and advances in early detection (*EPA, 2023*). However, radon exposure has become the leading cause of lung cancer in people who have never smoked ( *EPA, 2023; Mendez et al. 2011; Lagarde et al., 2001*). Radon is an airborne gas formed because of the emission of an alpha particle during radioactive decay; therefore, it will attach to other airborne particles and expose sensitive tissue to hazardous radioactivity. It is approximately 7.6 times denser than air and accumulates where ventilation is lacking (*Gillmore et al., 2010*). Recent studies also show a relationship between exposure to radon and breast cancer and skin cancer mortality (*Vienneau et al., 2017; Vopham et al., 2017*). In the past decade, the World Health Organization (WHO), launched an international radon project to increase awareness, collect data, and encourage prevention because no radon exposure treatments exist (*American Cancer Society, 2022; EPA, 2023*).

As radon production is related to the underlying geological conditions, mapping radon potential is fundamental for both awareness and prevention work. Previous maps used for public health work in the United States were based on regional bedrock geology, soil, airborne radiometry, housing stock data, and single radon hazard estimate for each

county (*Haneberg et al., 2020; Schumann, 1993*). Haneberg et al. (2020) created a geologically based statewide indoor-radon potential map of Kentucky by combining digital 1:24,000 bedrock geologic map coverage of the state (*Anderson et al., 2004; Cressman & Noger, 1981*) with 71,930 short-term radon home test kit results (Figure 1). Mapping radon in Kentucky is important because residents are at high risk of radon exposure due to the state's geological conditions, (*Chiavacci et al., 2020*). One of the biggest challenges in understanding geologic controls on radon distribution in Kentucky is that bedrock with the highest indoor radon potential, Mississippian Limestones, have low to moderate concentrations of uranium (*Phillips et al., 1993*). The Haneberg et al. (2020) map provides a visual representation of radon risk potential based on bedrock geologies that control radon emissions and, as a result, have the potential to reduce exposure and mortality rates (*Figure 1.1*). The map created by Haneberg, et al. (2020) using in-home detectors was produced at narrow, specific study area than typical surveys, but was highly dependent on the usage of the device by the homeowner which resulted in sparse point data. This narrow study area allowed for a more detailed survey at a near-surface level of data collection, producing a more detailed visualization of the radon levels in Kentucky given the proper usage of the homeowner.

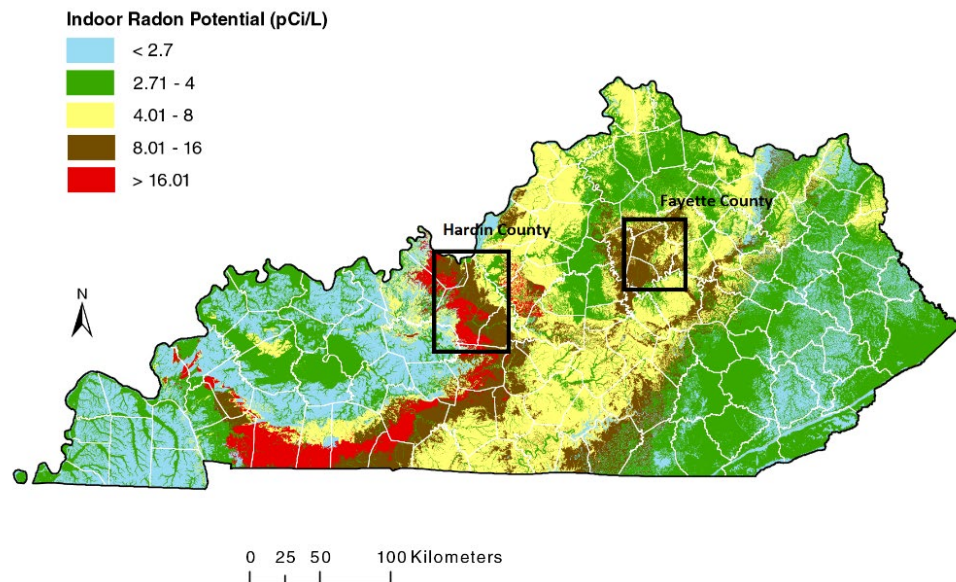


Figure 1.1 Indoor radon potential map created by the Kentucky Geological Survey; highlight of the main study areas of my project in Hardin County and Fayette County (statewide map from Haneberg et al., 2020).

Radon is a naturally occurring radioactive gas that is colorless, odorless, and typically disperses quickly into the atmosphere, and originates from the decay series of uranium-238 found in the earth's crust with a half-life  $4.5 \times 10^9$  years (*Al-Zoughool & Krewski, 2009*). The levels of uranium depend on the type of rocks and soil (*Al-Zoughool & Krewski, 2009; Muikku et al., 2007*) which contributes to the amount of radioactivity emitted into the atmosphere. Radon levels in the central Kentucky region are significantly high, with the average at 9.41 picocuries per liter (pCi/L) indoors, compared to the national average of 1.3pCi/L indoors (*Hadwick, 2014*) and 0.4 picocuries per liter (pCi/L) in the atmosphere (*EPA, 2023; EPA, 2022[b]*) in the United States. The EPA recommends home remediation in areas where the indoor radon level is between 2-4 pCi/L (*EPA, 2022[b]*).

Producing a geologically based indoor-radon potential survey map, Hahn et al. (2015) was able to determine that fourteen geologic formations analyzed in north central Kentucky had high average radon levels above the EPA-recommended action level. From surveys performed 25 years ago, Haneberg et al. (2020) showed that limestone and dolostone tend to have higher indoor-radon concentrations than siltstones and sandstones or unlithified surficial deposits. Mississippian limestones, Ordovician limestones, and Devonian black shales had the highest values in Kentucky and these values were weakly correlated to the mean aero-radiometric uranium concentrations (*Haneberg et al., 2020*). Production of geologically based radon maps is an effective way of communicating radon risk to residents throughout the United States since geologic data is widely available at varying resolutions (*Chiavacci et al., 2020*). It is critical to identify areas prone to high radon concentrations so interventions can be targeted to those at most risk (*Hahn et al., 2015*). These areas can be influenced by several factors including geology, ventilation, and groundwater, all of which can be surveyed with various methods. Radon maps fill a gap in knowledge about the hazard of radon and aid the avoidance of high-level exposure.

This study builds upon previous research on geologic controls of indoor radon in Kentucky (*Hahn et al., 2015; Haneberg et al., 2020*) by evaluating the suitability of a lightweight, uncrewed aerial vehicle (UAV) compatible gamma spectrometer for mapping the spatial distribution of soil radionuclides as a proxy for soil radon and, ultimately, indoor radon potential. During initial testing, we identified knowledge gaps related to the accuracy, precision, and sensitivity of the lightweight gamma spectrometer relative to its ability to collect data useful for radon potential mapping. Therefore, my work focused on understanding the relationship between spectrometer surveying height, sensitivity, on-

ground footprint size, and the parameters or factors that may affect the accuracy or precision of the spectrometer. The central hypothesis of this work is that radionuclide levels over different surfaces (soil, asphalt, rock type, faults, sinkholes, and karsts) will differ enough to be interpreted as separate ground types and signatures of geologic features could be detected by the lightweight, UAV-compatible spectrometer. Fieldwork was concentrated in two areas: the Inner Bluegrass region in Fayette County, Kentucky, and the Interior Mississippian Plateau region in Hardin County, Kentucky, which has indoor radon level readings of approximately 4.1-16.2 pCi/L or higher (*Figures 1.1, 1.2*).

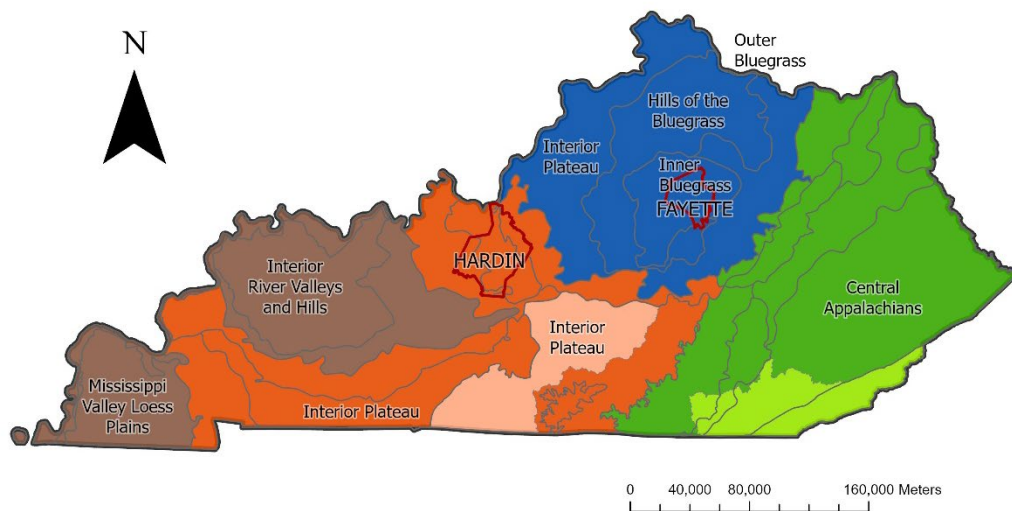


Figure 1.2 Map of the geographical regions of Kentucky used to understand the potential geologic control on the study area of the project. Data Source: Kentucky Cabinet of Transportation and Energy and Environment Cabinet.



## 1.1 Kentucky Geology and Indoor-Radon Potential

The near-surface geology in Kentucky (*Figure 1.3*) comprises primarily flat-lying limestone, shale, sandstone, siltstone, dolostone, and coal spanning ages from Ordovician to Pennsylvanian (*Haneberg et al., 2020; McDowell, 1986; McFarlan, 1943*). *Figure 1.3* is a visualization of the near surface geology in Kentucky created in ArcGIS Pro by Alexandria Thomas. The oldest exposed rocks in Kentucky, which were deposited during the Late Ordovician Period, are karstic limestones and shales that can incorporate uranium into the crystal structures of their mineral constituents (*Haneberg et al., 2020; Cressman, 1973; Karathanasis, 1991; McFarlan, 1943*). The Devonian System is comprised of black shale with high clay content and organic materials which contribute to their high traces of uranium. These Devonian rocks are also overlain by Lower Mississippian clay-rich shales, siltstones, and karstic limestones. During the Devonian Period, Kentucky was covered by shallow, tropical seas, and therefore, became a source of uranium content (*Swanson, 1961*). The uranium contents in the rocks are accumulated through a seawater reservoir which is highly effective for rapid transportation and distribution of minerals (*Swanson, 1961*). Formations in simplified geologic maps seem to correspond to aero-radiometric uranium concentrations in Kentucky, with the highest concentrations within the Devonian black shales, the median concentrations in the Ordovician Limestones and Quaternary alluvium deposits, and the lower concentrations in the unlithified clastic surficial deposits, sandstones, and siltstones (*Haneberg et al., 2020*). The Ohio Shale, a member of the Devonian System, and other black shales are typically recognized in the subsurface by their high gamma ray log values (*McDowell and Kepferle, 1986*). Black shales are rocks of widely differing origins, chemical compositions, mineralogical suites, grain sizes, colors, and other descriptive characteristics (*Swanson, 1961*). They are typically dark-colored, fine-grained, clastic sedimentary rocks that are abundant in disseminated, carbonaceous, organic matter that contributes to the color with a grain size of silt and clay. This rock type

is present in more than two hundred formations that were searched for uranium content in the United States (Swanson, 1961). Marine black shales are uniform in thickness and lithology over wide areas and contain marine fossils while nonmarine black shales are erratic in thickness and distribution interbedded with sandstones and plant coals (Swanson, 1961). All shales contain an average of 3-4 ppm of uranium falling between the range of 3 and 250 ppm individually, whereas thick marine shales contain an average of 20 ppm of uranium (Swanson, 1961). The organic matter content of the woody or humic type and soluble type are mechanisms for a mass fraction of uranium content in the Chattanooga Shale (Swanson, 1961). Phosphate is a common and distinct feature of black shales that contain 0.0001 – 0.1% uranium content per nodule, equaling 10% – 35% phosphorous pentoxide ( $P_2O_5$ ) content that heavy metal impurities such as radiotoxic uranium (Swanson, 1961; Mwalongo et al., 2022). Uranium levels in phosphate rocks can range from 10.7 mg/kg to 631.6 mg/kg depending on the type of phosphate in rocks (Mwalongo et al., 2022). There are at least fourteen factors that affect the uranium content in marine black shales; Swanson (1961) considered rock type, rate and type of weathering, rate of deposition, amount of organic matter present, and amount of phosphate present.

Karst development is particularly important in controlling radon distribution. This allows for rapid migration, trapping, and concentration of available radon gas (Currens, 2002). Karst is a type of landscape underlain by soluble rocks, in Kentucky limestone or dolostone, characterized by sinkholes, sinking streams, closed depressions, subterranean drainage, and caves (Currens, 2002). For perspective of the Kentucky karst landscape, 55% of Kentucky is underlain by rocks that could potentially develop karsts, 38% of Kentucky has some karst development, and 25% of Kentucky has well-developed karst features (Currens, 2002). The karst landscapes in Kentucky were developed on limestone over hundreds of thousands of years as the result of groundwater flow and dissolution of

soluble carbonate rocks. Researchers work to define key features of karst development that contribute to the uranium/radon concentration in Kentucky.

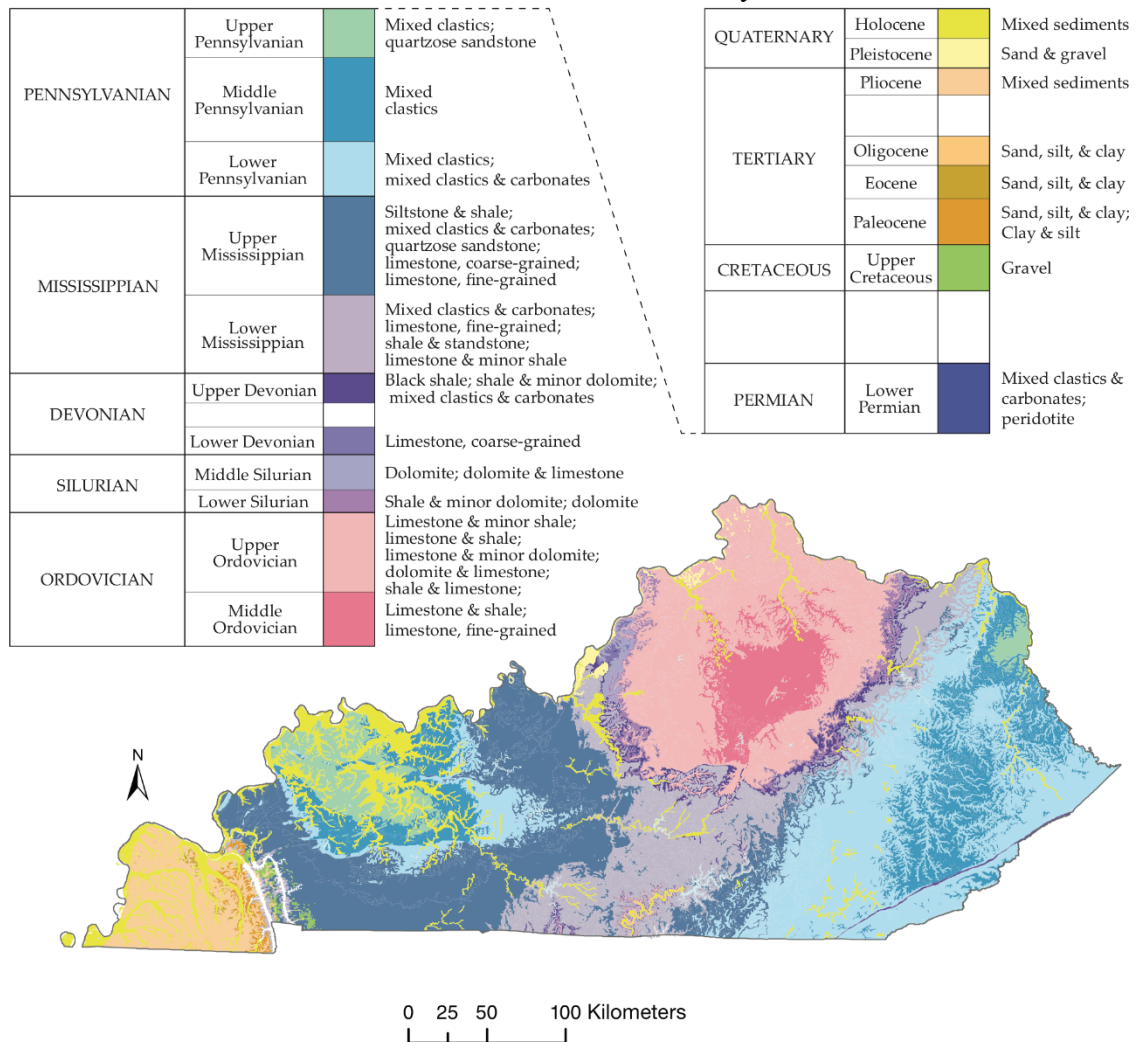


Figure 1.3 Near-surface geological map of Kentucky used to understand and visualize the lithology and other geological features that tend to affect uranium content. Data Source: Kentucky Geological Survey.

## 1.2 Previous Works

Some previous researchers have concluded that soil radon has seasonal variations that are typically greater over karstic limestone lithologies and less seasonal, but still elevated, over igneous lithologies (Gillmore *et al.*, 2010; Groves-Kirkby *et al.*, 2010). Increased levels of radon in soils near fractures and faults can be observed in the Himalayas

along the Dehar lineament and compared to lower levels in the other thrust zones and near the Himalayan Frontal Fault, perhaps indicating a buried or blind fault or thrust zone parallel to the Himalayan Frontal Fault (*Gillmore et al., 2010; Mahajan et al., 2010*). Another example is the Ravne Fault in Slovenia which has concentration levels ranging from 0.9 to 32.9 kBq/m<sup>3</sup> along deformation zones both perpendicular and parallel to the fault (*Gillmore et al., 2010; Vaupotic et al., 2010*). Variations of radon in time and space influence concentration and emission level and indicate how cyclic and anomalous features are analyzed (*Gillmore et al., 2010; Kahn et al., 1990; Planinic et al., 2000*). Radon has been used to monitor earthquake activity in places like the Anatolian Faults in Turkey (*Gillmore, 1999; Gillmore et al. 2010; Baykara et al., 2009; Inan et al., 2008*). Researchers have also observed high levels of radon in work environments like tunnels, caves, and mines throughout the world (*Baykara et al., 2009; Inan et al., 2008*). Major effects on radon generation and accumulation include the underlying geology like granites and metamorphic or sedimentary carbonate limestones.

Other studies have used aero-radiometric surveys to map thorium, potassium, and uranium bearing minerals (*Philips et al., 1993*). These types of surveys can provide targets for drilling exploration, facilitate more accurate assessments of overall trends in bedrock geochemistry, and improve our understanding of near surface to crustal geologic processes. Aero-radiometric surveys may be a powerful way to image areas of in situ radon potential, provide insights into relations to specific geomorphic features, transport pathways, and provenance, highlight the importance of processes in concentrating sediments, and implications for further developing an understanding of the broader geologic processes associated with important deposits (*Shah et al., 2021*). Over the past few years, satellite data (*Aydar & Diker, 2021*) were used for radon detection over a large area, but tended to have low resolution, therefore, airborne radiometric surveys were conducted to narrow the survey area and collect more data points for increased resolution.

To reduce the influence of background radiation, steel shields were attached to large airborne spectrometers as a blocking agent to the radioactive wave emission. This is not feasible with smaller spectrometers because of the limited payload of small UAVs. At the time of this study, only two manufacturers offered lightweight gamma spectrometers for environmental mapping. These two are Terraplus®, which was used for this project, and Medusa®. Terraplus® was chosen based on cost and availability. It was new, unstudied technology. The Medusa® spectrometer has at least two pre-existing publications on its functionality and is foundational for our framework development of the project (*Veeke et al., 2021, a & b*) Veeke et al. (2021a.b) used an APID One UAV manufactured by MainBase in Linköping, Sweden along with three Medusa spectrometers with an MS-2000 Agri detector of 12 kg containing a 2000 ml CsI/Na scintillation crystal, an MS-1000 Drone-borne detector of 7 kg containing a 1000 ml CsI/Tl scintillation crystal, and an MS-350 Ultralight drone detector at 2.2 kg containing a 350 ml CsI/Tl scintillation crystal, lidar scanner, GPS, and barometer to accurately measure the machine's position and height. The test sites were rectangular areas on a field with spatial variability, no high obstacles, and transition zones between postglacial fine sand and clay sediments (*Veeke et al., 2021[a]*). The gamma spectrometers collected the total number of detected counts during each time interval to determine the minimal practical detector size of a UAV-borne gamma-ray spectrometer while still providing accurate information of <sup>40</sup>K, <sup>238</sup>U, and <sup>232</sup>Th. Another study by Veeke et al. (2021) [b] done with the same instrument setup mentioned above was developed to measure radionuclide concentrations operating at heights between 0 and 40 meters in a stationary position and provides analytical, computational, and experimental height corrections. The study presented a footprint and height correction as a function of the change in height. It is known that the footprint increases with the increase in height and determines the spatial resolution of the airborne survey and is recommended to fly at a height where the footprint includes 65-95% of the radiation (*Veeke et al., 2021[b]*).

## CHAPTER 2. BACKGROUND

### 2.1 Radon Geochemistry

Radon ( $^{222}\text{Rn}$ ) is an odorless, colorless, radioactive gas that forms naturally from the radioactive decay of uranium, thorium, or radium within rocks, soil, and groundwater and is released into the atmosphere (*EPA, 2023; EPA, 2022*). The first element in the decay series of radium and radon is  $^{238}\text{U}$ , the parent of the two daughters, with a half-life of 4.4 billion years. One picocurie is equal to two alpha decays per minute; therefore 4 pCi/L, the indoor radon level recommended for home remediation, is equal to 8 alpha decays per minute per liter of air. Outdoor levels of radon in air range from  $< 0.1$  pCi/L to 30 pCi/L, which averages to about 0.2 pCi/L in the atmosphere, while soils contain between 20 pCi/L and 100,000 pCi/L of radon, averaging between 200 and 2,000 pCi/L in soil air (*Otton, 1992*). Geologic conditions, including soil and bedrock type, govern the occurrence of uranium, the formation of radon, and the movement of atoms causing radon levels to vary greatly between indoor air, outdoor air, and soil air. Most rocks contain at least a small amount of uranium which determines the uranium content of the overlying soil. Rocks that have higher than average uranium content are light-colored volcanic rocks, granites, dark shales, sedimentary rocks with phosphate, and metamorphic rocks derived from the previous rocks which may contain approximately 100 parts per million uranium along with traces of radon being present (*Otton, 1992*).

Figure 2.1 displays the process of solid radium ( $^{226}\text{Ra}$ ) decay, the daughter product of uranium ( $^{238}\text{U}$ ), as it forms and ejects an alpha ( $\alpha$ ) particle, which is the loss of two protons and two neutrons (*Gilmore et al., 2010*). Alpha particles aid in the formation of the radon atom with a half-life of 3.8 days. Radon atoms recoil in the opposite direction from

alpha particles, entering pores or fractures in the rock (*Otton, 1992*) (*Figure 2.1*). The direction of the recoil is an important factor affecting the release of radon from mineral grains (*Otton, 1992*). The location of the radium atom in the mineral and the direction of the recoil of the radon atom determines if the radon atom enters a pore space, crosses all the way through the pore space, and embeds itself in a mineral grain, or moves slowly through the pore space if the rock is saturated with water.

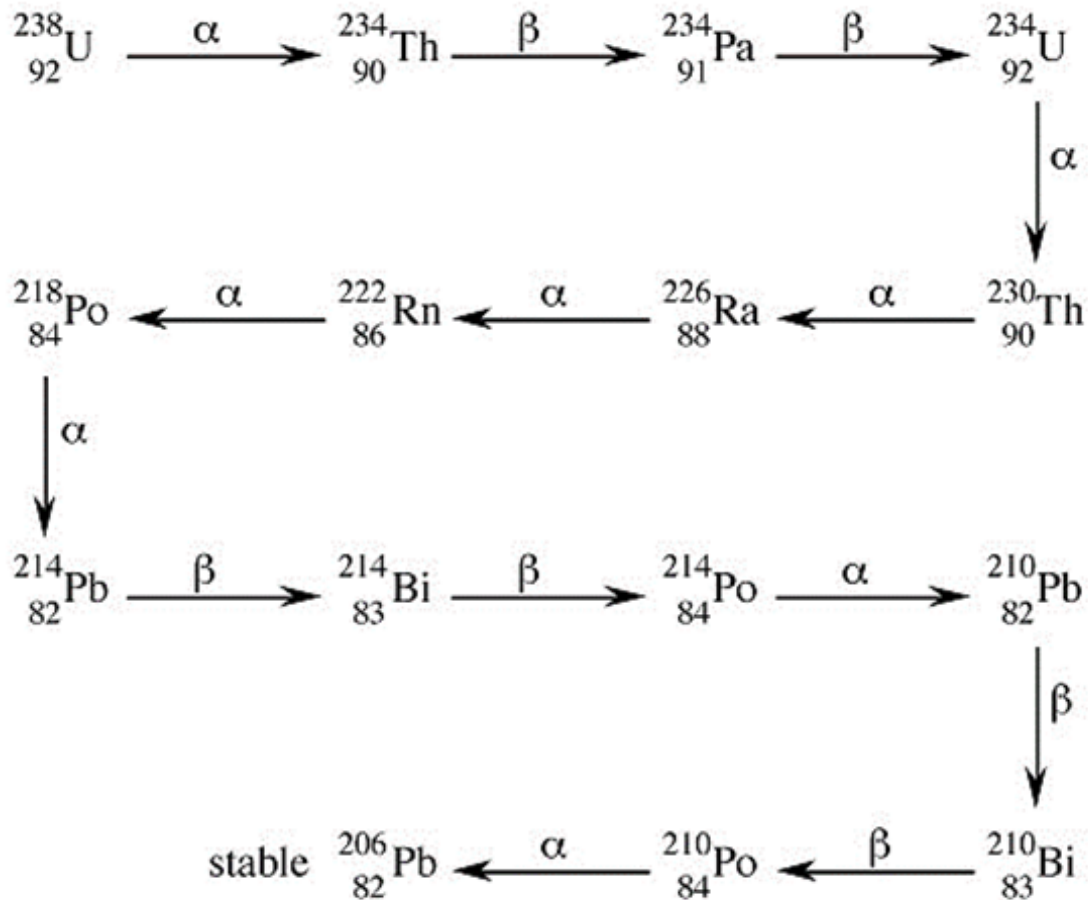


Figure 2.1 Diagram of decay series for radon from Uranium 238 (*Barron, 2011*).

Between 10% and 50% of the radon atoms produced escape the mineral grain and enter the pore space (*Otton, 1992*). Due to its gaseous state, radon has greater mobility than

uranium and radium, so it can easily escape rocks and soils through fractures and openings into the pore spaces of the rocks, soils and into the atmosphere. The method and speed of radon atoms are dependent on the soil or rock moisture content, porosity, and permeability (*Otton, 1992*). Lakes and rivers have low levels of radon due to the atom's ability to escape into the air, but the underlying rock can influence the levels in the water, especially phosphatic rocks (*Otton, 1992*). Higher levels of radon occur in groundwater overlain by granites, dark shales, phosphatic limestones, or arkosic sandstones due to lower accessibility to the air (*Otton, 1992*). Cooler temperatures enter through the soil and restrict the emission of radon from the soil by creating a barrier through the toughening of soil or the production of snow or other frozen precipitation. The temperature of the environment affects the rate of emission of the alpha particle being lower in cooler temperatures, therefore lowering the measurement analyzed by the spectrometer. More space and interconnectedness in rocks and soil along with warmer temperature environments lead to the material being drier creating more movement distance and allowing for concentrations to lay between the range of 20 and 2,000 pCi/L (*Figure 2.2*) (*Otton, 1992*). Knowledge about the geology of the sites studied in the Central Kentucky Region and its radon potential based on specific bedrock or soil types can help develop an understanding of the concentration of the gas particles within those materials. The radon potential of a site is evaluated using data from uranium or radium content of soils and underlying rocks and the permeability and moisture content of the soils as well as information from geologic maps, maps of surface radioactivity, and soil maps (*Figure 2.2*) (*Otton, 1992*). Geologic maps indicate a general level of uranium or radium expected in the rocks and soils in the area, by showing where rocks with high levels of uranium occur and providing key information



for understanding radon levels of surficial materials in correlation to the physical properties of near-surface materials. Investigating radon migration through and between the atmosphere, hydrosphere, lithosphere, and biosphere can lead to understanding the mechanisms involved with other natural hazards, such as earthquakes and volcanic eruptions to monitor, prevent, and protect humans from radioactive exposure through the increase of knowledge (Gillmore *et al.*, 2010).

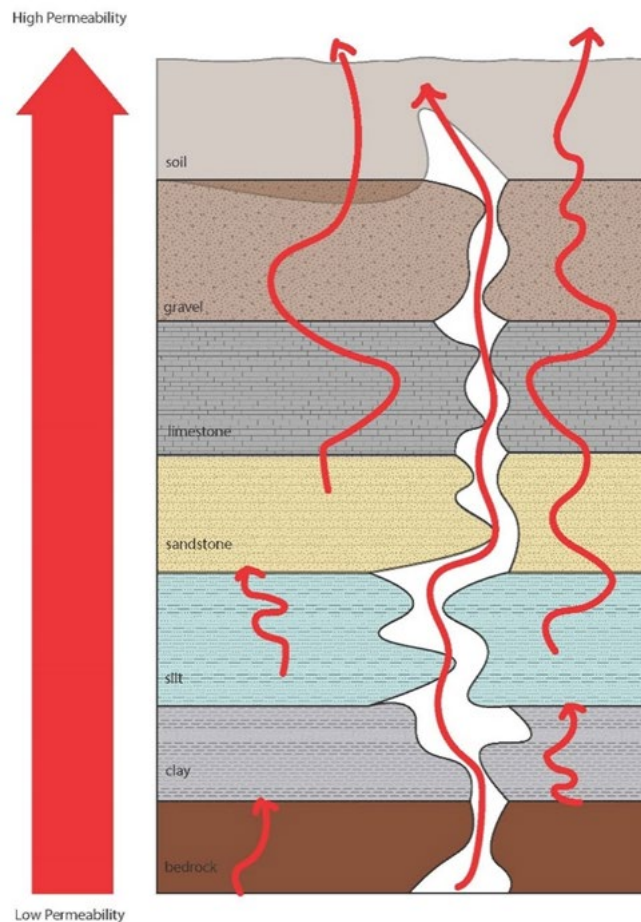


Figure 2.2 Permeability sketch of different rock types ranked from low permeability (bottom) to high permeability (top). The white space within the bedrock layers represents a fracture, that allows for a more direct and therefore more rapid path for the particles to take. Adapted from a figure in Otton, 1992.

## 2.2 Study Area

My work, the analysis of a UAV spectrometer to contribute to the future analysis of radon, was conducted in the central lowland region of Kentucky referred to as the Bluegrass Region (*Figure 2.3*) comprised of formations of Ordovician, Silurian, and Mid-Devonian rocks because of the history of high indoor radon potential levels (*Haneberg et al., 2020*). This area has a range of karst development maturity, which is determined by limestone type, mineral composition, and bedding thickness (*Kentucky Geological Survey Interactive Geologic Map, 2020*). The Inner Bluegrass region is the most central portion of Kentucky and contains 30% of the highly phosphatic Lexington Limestone and Cynthiana Limestone (*McFarlan, 1944*). The maximum development of the Bluegrass Region is a result of the lower regional dip with variable amounts of alluvial deposits along main streams.

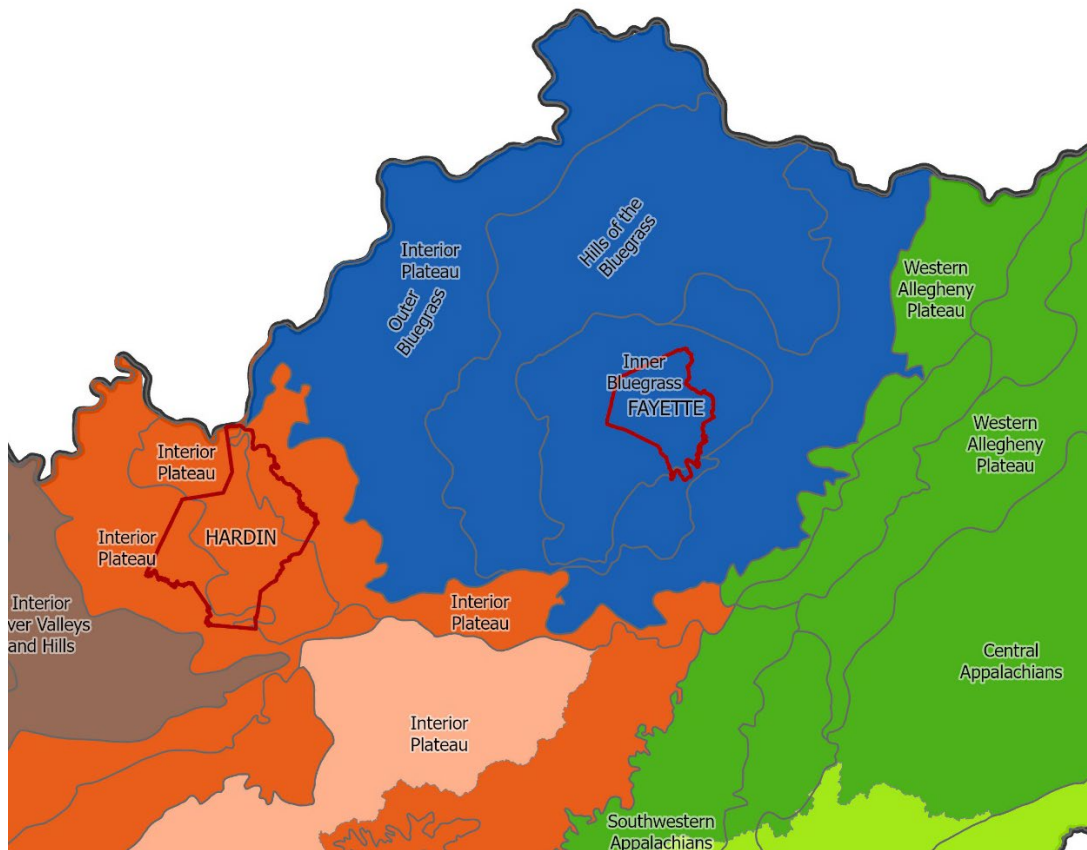


Figure 2.3 Geographical regions of the study areas for the project highlighting the Inner Bluegrass (blue) for many of the surveys and the Interior Mississippian Plateau (orange) for one of the surveys. Data Source: Kentucky Cabinet of Transportation and Energy and Environment Cabinet.

The Ordovician system in Kentucky is overlain disconformably to paraconformably by the Silurian-aged rocks (*McDowell, Cressman, and Peterson, 1986*). The Inner Bluegrass is underlain by Middle Ordovician strata comprising primarily Lexington Limestone, which is a fossiliferous and fossil fragmental calcarenite, while the Outer Bluegrass is underlain by an Upper Ordovician sequence of interbedded fossiliferous limestones, dolomites, and shales (*McDowell, Cressman, and Peterson, 1986; Cressman, 1973; Black, Cressman, and MacQuown, 1965*). The Lexington Limestone is limited to the

Inner Bluegrass region (*Figure 2.3*) and comprised of 12 members. It is approximately 98 m thick extending 16 km north of Frankfort and east towards Georgetown and Paris, and thins to the north, west, and south because of the integration of the Clays Ferry Formation laterally by splitting them into thin sections that individually wedge out (*McDowell, Cressman, and Peterson, 1986; Cressman, 1973*).

Sites in this study are underlain by the Tanglewood Limestone member, one of the 12 members within the Lexington Limestone, which is an irregular body of fossil-fragmented calcarenite making up a majority of the upper Lexington Limestone (*Cressman, 1973; Black et al., 1965*). It meets with the Clays Ferry Formation and is made up of well-sorted and crossbedded calcarenite with phosphate grains that have been reworked, rounded, sorted, and concentrated by currents (*McDowell, Cressman, and Peterson, 1986*). The Tanglewood is a pinkish grey, medium-grained, well-sorted bioclastic calcarenite of planar or wavy bedding ranging from 0.2-1 ft in thickness containing approximately 2.4 % phosphorous pentoxide (P<sub>2</sub>O<sub>5</sub>) within phosphatic laminae from < 1-5 mm thick. The overall mineral composition is 74% calcite, 13% dolomite, 6% apatite, and 5% quartz and clay, and the overall thickness of the formation ranges from 60-100ft (*Cressman, 1973*).

The upper part of the Ordovician System in central Kentucky consists of mostly limestones with a small percentage of fossils and fossil-fragmented matrices and mostly shales but includes siltstone, dolomite, and mudstone. The limestones are a medium grey and weather to olive-grey, yellowish-grey, or brown while the shales are a highly calcareous, silty, fissile, fossiliferous greenish grey or olive grey which weathers to a yellowish grey (*McDowell, Cressman, and Peterson, 1986*). For this study, the Garrard

Siltstone and Clays Ferry Formations were the two formations observed within this system. The Clays Ferry Formation is approximately 27-91 m thick of interbedded limestone and shale and the Garrard Siltstone is 0-30 m thick in the southeastern part of the main outcrop of the uppermost part of interbedded siltstone, shale, and limestone (*McDowell, Cressman, and Peterson, 1986*). The Clays Ferry Formation contains 30-60% limestone in 1-6 thick beds (*Cressman, 1973; Weir and Green, 1965*). It is medium to dark grey argillaceous calcisiltite, medium grey brachiopod-bearing limestone, and medium grey crinoid-bearing calcarenite with an overall mineral composition of 1.5% apatite, 43% calcite, 9% dolomite, and 44% quartz and clay (*Cressman, 1973*).

Lastly, the Devonian rocks in this study area are dominated by black shale. The New Albany Shale is a member of the system that is organic black shale with thin beds of greenish-grey shale near the top and base (*McDowell and Kepferle, 1986*). This member is approximately 34 m thick or Upper Devonian, Middle Devonian, and Early Mississippian fossiliferous rock that is continuous with the Chattanooga Shale (*McDowell and Kepferle, 1986*). The Devonian shales occur primarily in the western regions of Kentucky, outside of the main study area. While there were no Devonian black shales in the study areas' data, it is important to recognize this rock type has consistently high uranium content, therefore increasing radon potential in the surface materials and atmosphere.

Karst is a landscape produced by the dissolution of soluble bedrock. It is being researched as a potential impact on the uranium content and the release of radon into the atmosphere. Kentucky is one of the world's most famous karst areas, with the Inner Bluegrass region being the 2nd largest karst region in Kentucky. With indoor radon potential measuring high in regions common for karst development, it is important to

compare the potential for in situ radon emissions from soils and rocks underlain by similar karst features. The correlation between karst development and soil radon emissions is the subject of ongoing research in the scientific community. The limestone within this study area has given rise to a well-developed karst landscape.

Hardin County lies within the Interior Mississippian Plateaus physiographic region, which differs from the Inner Bluegrass physiographic region (*Figure 1.2*). There are different bedrock formations within the plateau, including the Upper Mississippian St. Louis Limestone (*Figure 1.3*). The St. Louis Limestone is characterized by medium to thick-bedded, coarse-grained, crinoidal, cross-bedded cherty limestone of medium or black color. Some formations exhibit thin beds of limestone and shale (*McFarlan, 1944*). In Hardin County, the St. Louis limestone is earthy, siliceous geode bearing beds with the top 3 meters full of black flint (*McFarlan, 1944*). This formation also includes large quantities of compact yellowish chert with a chalky texture. The Interior Mississippian Plateaus form a broad belt to the west and south of the Bluegrass region. This region includes a limestone succession of St. Louis limestone, Ste. Genevieve limestone, and Chester limestone. Within the region is the Pennyryle (or Pennyroyal) Plateau, which is defined by slope pairs developed on the outward-dipping St. Louis Limestone at the base and the Mammoth Cave Plateau at the top (*McFarlan, 1944*). The Pennyryle Plateau has small local relief with karst topography, limestone sinks, and inferior soil compared to the Bluegrass region (*McFarlan, 1944*).

### 2.3 Spectrometer and UAV

Gamma-ray spectroscopy is the study of the emissions of photons that are identifiable between different elements and isotopes while having a higher energy than

optical spectroscopy. A gamma-ray spectrometer is an instrument used to measure the spectrum of the intensity of gamma radiation against the energy of each photon through the collection and observation of the data. The data is observed by counting individual photons from different directions and distances from the instrument. If there are no obstructions, the machine can collect continuous data. Large spectrometers have been used to study radioactivity of entire states or countries for over 50 years, but the data produces lower resolution and coverage. This can be combated by producing high resolution and coverage data with an instrument that can be used closer to ground level over large areas. Duval et al. (2009) and Duval et al. (1971) describe an early application of mapping based on airborne gamma ray spectrometry. Each measurement samples an area of several thousand square meters to a depth of about 30 cm (Duval et al., 2009; Duval, Cook, and Adams, 1971). The measurements for Kentucky are 0.5-1.7% of potassium, 1.3-2.3 ppm of uranium, 4.6-7.9 ppm of thorium, 28-52 nGy/hour of gamma-ray absorbed dose, and 42-48 nGy/hour of cosmic ray exposure within a 114-791 m of digital topography (Duval et al., 2009).

Modern technology has allowed the development of smaller, UAV-compatible spectrometers (Figure 2.4) that may have the potential to be used for soil radon mapping. Traditionally, aspects like faults and sinkholes were not considered to have an effect on radon potential given the knowledge of the influence of rock type. Because we know UAV-based spectrometer surveys yield good results, and we have drones that may be able to be flown over areas that were not considered in the past, we can explore low-level radioactivity. Stationary spectrometers with NaI/Tl dosimeters have been used in the past to measure outdoor concentrations of  $^{238}\text{U}$  series,  $^{232}\text{Th}$  series,  $^{40}\text{K}$ , and other terrestrial

radionuclides in soil, agricultural raw materials, forestry products, and construction materials (Ramzeav *et al.*, 2017; International Atomic Energy Agency, 1999). Stationary spectrometers took a direct measurement of the gamma dose rate in the air to assess external exposure to humans. The method was developed according to theoretical principles of in situ gamma-ray spectrometry and demonstrated that it could provide more representative data for the evaluation of gamma dose rate in the air rather than from a soil sample (Ramzeav *et al.*, 2017; Beck *et al.*, 1964; Beck *et al.*, 1972). The NaI/Tl detector is a cylindrical scintillation with an energy resolution of 7.3% and each energy window was centered on the 40K peaks, 214B peak, and the 208Tl peak to estimate the activity concentrations of 40K, 238U, and 232Th (Ramzeav *et al.*, 2017). The results from the study with the stationary NaI/Tl detector confirm the applicability of in situ gamma-ray spectrometry and the technology has expanded since. Other studies of in situ concentration have led to the development of maps based on sediment contamination to assess the strong geochemical and geophysical correlations to the radioactive concentrations (Graaf *et al.*, 2007). Background radiation is always present in the environment, including the Sun, stars, Earth, and all living things. To possibly evaluate the true emission of radon from the study area, a shielding method might have been necessary to isolate the uranium, thorium, and potassium particles in the area (EPA, 2022[a]). Background radiation levels change with the change in the environment such as location and weather (EPA, 2022[a]). Weather such as snow and rain can shield or wash out the background radiation of any given environment (EPA, 2022[a]).



### 2.3.1 Instrumentation

For this study, a DJI Matrice 600 Pro unmanned aerial vehicle (UAV) (*Figure 2.4*) was chosen and modified with mounting brackets to specifically carry the load of a UAV-compatible spectrometer (*Figure 2.5*) because that UAV is well known for surveying commercially and can carry the payload of the spectrometer. The UAV was designed for professional aerial industrial applications and built to integrate the A3 flight controller, Lightbridge transmission system, and intelligent batteries and battery management system for maximum performance and efficient setup (*DJI, 2023*). The dimensions of the unfolded UAV, including the propellers, frame arms, and GPS mount, are 1668 mm x 1518 mm x 759 mm with an overall weight ranging from 9.1-9.6 kg including the batteries, and can carry 15.1 kg at takeoff (*Figure 2.4, right*). The drone and the batteries can withstand temperatures ranging from 14 degrees to 104 degrees Fahrenheit which we used as limitations on safety as well as the effect on data. Its maximum speed is 18 meters per second with a max wind resistance of 8 meters per second and a max altitude of 2500 meters.



Figure 2.4 The DJI Matrice 600 Pro, an unmanned aerial vehicle (UAV), mid-flight (left) and ground bound (right).

The instrument used for this study counts uranium, thorium, potassium, and additionally calculates the total count of all three elements. The GEORADiS® D230A spectrometer with serial number 007 was specifically designed for UAV applications (*Figure 2.5*) (*Terraplus, 2020*). This instrument uses two, 1024 channel gamma-ray spectrometers with four NaI/Tl detectors, small data acquisition, and a control unit. The spectrometer uses an SD card for data storage and a user interface accessible through a laptop or desktop personal computer using a software package that comes with the instrument. The spectrometer is housed in a lightweight thin aluminum casing, includes a small Li-Ion battery for 4 hours of operation, and includes 4 hoisting points to be connected to the spectrometer. The package comes with a GPS module that can be mounted via cable to the top of the instrument. This 3.5 kg, 145mm x 78 mm x 260 mm spectrometer can operate in environments ranging from -10 C to +50 C (*Terraplus, 2020*). There are at least two known drone-compatible gamma spectrometers, but the GEORADiS® D230A was chosen on the basis of costs and delivery time. For this project, we conducted four testing methods to understand the precision and sensitivity of the GEORADiS® D230A (*Figure 2.5*) spectrometer and two kinds of tests to document how geologic features, namely faults and sinkholes, affect spectrometer survey results.



Figure 2.5 The GEORADiS® D230 gamma-ray spectrometer with a NaI/Tl crystal detector.

## CHAPTER 3. METHODS

### 3.1 Overview

The four methods for analyzing the precision and sensitivity of the spectrometer were (1) a series of stationary tests, (2) flights over one surface type or bedrock material, (3) flights over two surface types or bedrock materials, and (4) flights over three surface types or bedrock materials. The two methods for analyzing the potential effect of geology on the results are walking surveys over known fault divisions and walking surveys over known sinkholes. These methods yielded ten sets of results. A new group number is established every time the unit was started and stopped for data collection.

The total count measured by the spectrometer is different from the frequency calculated through statistics. Total count is the total amount of photon at a specific point that the spectrometer recognized. The frequency is the amount of time the total count of a given point occurs within the data. The frequency range changes for each histogram because the number of points the spectrometer collects changes based on time, surface material, and the machine determining if a point is relevant or not. The machine determination variable is not controlled by the user.

For this project, a gamma spectrometer and a small UAV were used to record uranium, thorium, and potassium at each field site. We completed several multi-altitude flights and near-ground surveys carrying the spectrometer by hand in simple (single material areas, i.e., one rock type or one surface material) and complex (multiple material areas, i.e., transitions between different surface materials or different rock types) surface material conditions. Statistical analysis was also conducted to characterize background

levels and establish limits to detect subsurface geology by completing surveys over known faults and sinkholes within the central Kentucky area to see if there are detectable anomalies. As opposed to typical aero-radiometric surveys, my surveys are conducted at a height of one meter to tens of meters above the ground and are site specific. As opposed to all other detection tests done in the past, this level of surveying is to understand how precise this method is since it is small-scale and collects many data points. At each collection site, the spectrometer was carried by hand or flown at heights ranging from ground level to 40 meters above ground level to document changes in spectrometer sensitivity as a function of survey height. The UAV flights are planned using software called UgCS by SPH Engineering (*Figure 3.1*). The controller connects to the UAV via Bluetooth and transfers the flight plan to enable autopilot mode. The flight plan of four flights was conducted at 5 meters, 10 meters, 20 meters, and 40 meters above ground level at 2-5 m/s. Walking surveys following the same path as the flight plan were performed holding the spectrometer 1-meter height above ground level.



Figure 3.1 UgCS software by SPH Engineering used to plan flights at each location (Location 3 pictured) (SPH Engineering, 2023).

The field research was in six different locations in the central Kentucky Inner Bluegrass region. Location 1 (latitude 38.03438762827302, longitude -84.5025779361404), near the Mining and Minerals Resources Building on the University of Kentucky campus, was chosen for accessibility to the three different surface materials (soil, asphalt, and concrete) for the stationary and walking survey field tests at 1-meter and 1.2-meter height above ground level. Location 2 (latitude 37.98933000756201, longitude -84.41935445081484), at Jacobson Park in Lexington, Kentucky was chosen for its relatively flat terrain, accessibility to areas with soil and asphalt ground covering, and a lack of obstruction from tall trees and buildings. Walking and flight survey field tests were conducted at 1 m, 5 m, 20 m, and 40 m heights at a speed of 5 m/s for flights above 1 m. The 1-m handheld surveys were performed at a 0.30 m/s walking pace. The flight speed was changed at location 3 after discovering an initial complication with the UAV at location 2. Location 3 (latitude 38.136879441408595, longitude -84.5078788104715), on World Games Way, is located off the KY-1973, or Iron Works Pike, as a turn-off lane to Research Park Drive in northern Lexington, Kentucky near the Kentucky Horse Park Campground. This location was chosen for its relatively flat terrain, accessibility to areas covered by both soil and asphalt, and a lack of obstruction from tall trees and buildings for flight surveys conducted at 5 m, 10 m, 20 m, and 40 m above ground level at 2 m/s. Location 4 (latitude 38.13897336923546, longitude -84.51444551181821), at Berea Road Soccer Complex, is located on Berea Road off the KY-1973 or Iron Works Pike in Lexington, Kentucky. This location was chosen for the accessibility to relatively flat floodplain terrain that lacks obstruction from tall trees and buildings for stationary, walking, and flight surveys at 1 m, 5 m, 10 m, 20 m and 40 m above ground level (*Table*

3.1). Location 5 is near Hickory Lane on private property outside of Fort Knox, Hardin County, Kentucky. This location was chosen for accessibility to a sinkhole without a tree or building obstructions for two walking surveys at 1.2 meters above ground level to cover the area of each sinkhole. The last location, location 6 (latitude 38.006092628348085, longitude -84.48449175514442 to latitude 38.00122205807263, longitude -84.47754751609003), is along Alumni Drive from Chinoe Road to Lakeside Drive in Lexington, Kentucky. Location 6, which comprises two linear out-and-back survey lines, was chosen to transect three bedrock units separated by two faults shown on the published 1:24,000 bedrock geologic map of the area (*Figure 3.2*). The Hardin County and Alumni Drive location was walked because the UAV was being repaired from a flight gone wrong for separate project. Tests at the first four locations were a part of the process to analyze the precision and sensitivity of the UAV-mountable gamma spectrometer while the last two locations were to learn whether the instrument is sensitive enough to record distinct signatures over geologic features like faults and sinkholes. These areas were selected based on easy access and mapped bedrock geology. The data collected from the unit is displayed as photon counts of uranium, thorium, potassium, and total counts.

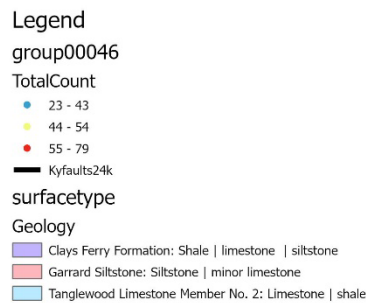
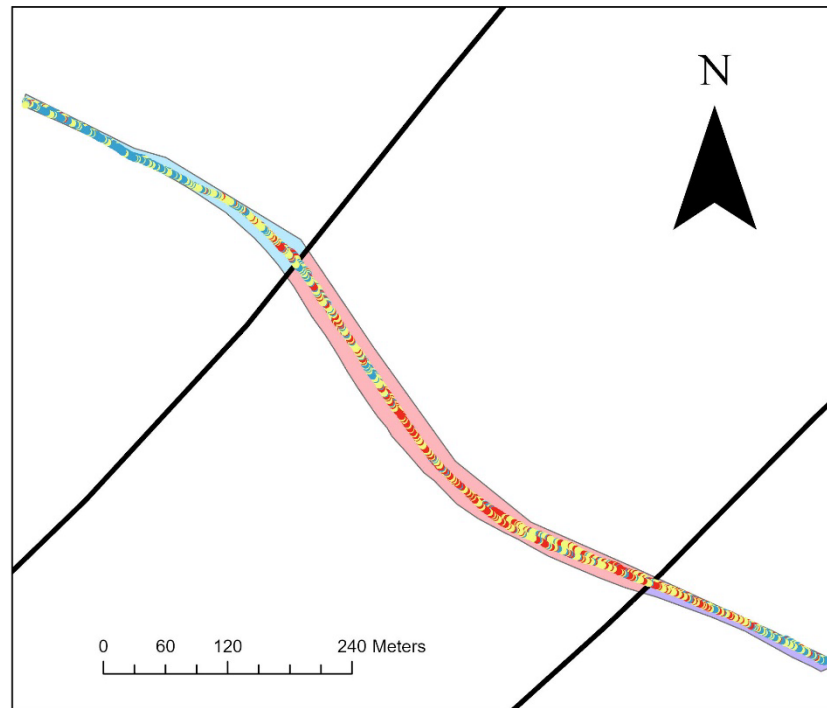


Figure 3.2 Fault map created by Alexandria Thomas of the transect along at Location 6. Data Source: Kentucky Geological Survey

The data collected was processed using the application MakeD into a table showing the uranium, thorium, and potassium and the total counts. MakeD is a geophysical processing application that manipulates raw data of photon counts collected from the spectrometer through the application of algorithms and transforms to make the wanted information concise in time and frequency domains. The counts from the table are converted to point values in ArcGIS Pro and are used to produce statistics of the total count



in RStudio (*Table 3.1*). ArcGIS Pro is a geographic information system that creates, manages, analyzes, and maps data from a visual perspective that was created by the company Esri. RStudio is an integrated development environment for R which is a programming language for statistical computing and graphics. Sub-hypotheses produced from these methods are (a) shielding will limit the background radiation, (b) measuring for longer periods of time will not significantly impact the average total count, (c) increasing height above the ground will increase the footprint and total count result, and (d) we can detect changes in rock type and/or the presence of geologic features like fault or sinkholes and determine the limit of sensitivity the spectrometer to detect those changes or features.

Table 3.1 This is a constructed from the statistics produced in RStudio for each flight plan of a grid of one material at multiple elevations. Each group represents the start and stop of the instrument for each grid or stationary test. The unit for each statistic is counts.

<b>Grid one-Material (multi-elevation)</b>	<b>Minimum (counts)</b>	<b>1<sup>st</sup> Quartile (counts)</b>	<b>Median (counts)</b>	<b>Mean (counts)</b>	<b>3<sup>rd</sup> Quartile (counts)</b>	<b>Maximum (counts)</b>	<b>Standard Deviation (counts)</b>
group 00033 (1m)	23.00	35.00	39.00	39.76	44.00	63.00	6.610392
group 00029 (10m)	21.00	38.00	43.00	43.28	48.00	66.00	7.588081
group 00028 (20m)	23.00	36.00	41.00	41.43	46.00	66.00	7.560931
group 00030 (40m)	23.00	31.00	36.00	37.83	43.00	64.00	8.767917

## CHAPTER 4. RESULTS

### 4.1 Results

#### 4.1.1 GPS Reliability – Stationary Test

A stationary test was conducted to analyze the stability of the GPS data from the unit without further post-processing. At Berea Road Soccer Complex, these tests were conducted in the same location at a fencepost in the complex between the parking lot and the soccer fields on the soil. There is a slight increase in total counts between each group, which means more latitude/longitude pairs were collected, due to the larger amount of time it ran, but their statistics are otherwise similar. Before conducting a grid flight plan above ground level, a final stationary test was performed at the home location (the starting point before the initial waypoint on the mapped grid for the flight), resulting in a mean value, total count value and frequency range that is lower due to the shorter amount of time it sat in this position. Overall, each stationary test's statistical information was similar. The raw location shows an expectable level of GPS variability within each data set (roughly +/- 2m) and drifts in the GPS system in the roughly 2 hours between the two initial data set collections. This expectable level is determined from comparing the GPS results of the spectrometer to the location coordinates in Google Maps or Apple Maps. The GPS reliability proved to be acceptable through multiple stationary tests. Groups 19 and 24 were the two stationary tests described above at this research location. A table of each point collected from the spectrometer was produced using the geoprocessing system MakeD by inputting a meas\_log.csv file, inputting groups 24 and 19 as a comma-separated values file using the command "group00024.csv", inputting the flight number as the same group

number, and it generates the data as a table that can be opened with Excel. While these were stationary tests, the MakeD program labels the group number header as flight number in the coding interface. The initial table is edited to condense the information to only display the counts from the uranium, thorium, potassium, and total count. This new table is imported into RStudio (*Appendix*).

Table 4.1 This shows the data statistics of the GPS reliability test conducted to understand the parameters of the spectrometer.

GPS Reliability	Minimum (counts)	1st Quartile (counts)	Median (counts)	Mean (counts)	3rd Quartile (counts)	Maximum (counts)	Standard Deviation (counts)
group 00019	32.00	50.00	55.00	55.00	60.00	78.00	7.130670
group 00024	34.00	50.00	55.00	55.09	60.00	83.00	7.399433

Figure 4.1 is a 2D map that was created to visualize the variability of locations obtained from the GPS unit on the spectrometer. The commands in RStudio in Table 4.1 produced show for group 19 the minimum of total count frequency of 32, the 1st quartile of total count frequency of 50, the median of total count of 55, the 3rd quartile of total count frequency of 60, the maximum of total count frequency of 78, and the standard deviation of total count frequency of  $\pm 7.1$ . A table for group 24 was also produced showing the minimum of total count frequency of 34, the 1st quartile of total count frequency of 50, the median of total count of 55, the 3rd quartile of total count frequency of 60, the maximum of total count frequency of 83, and the standard deviation of total count frequency of  $\pm 7.4$  (*Table 4.1*).

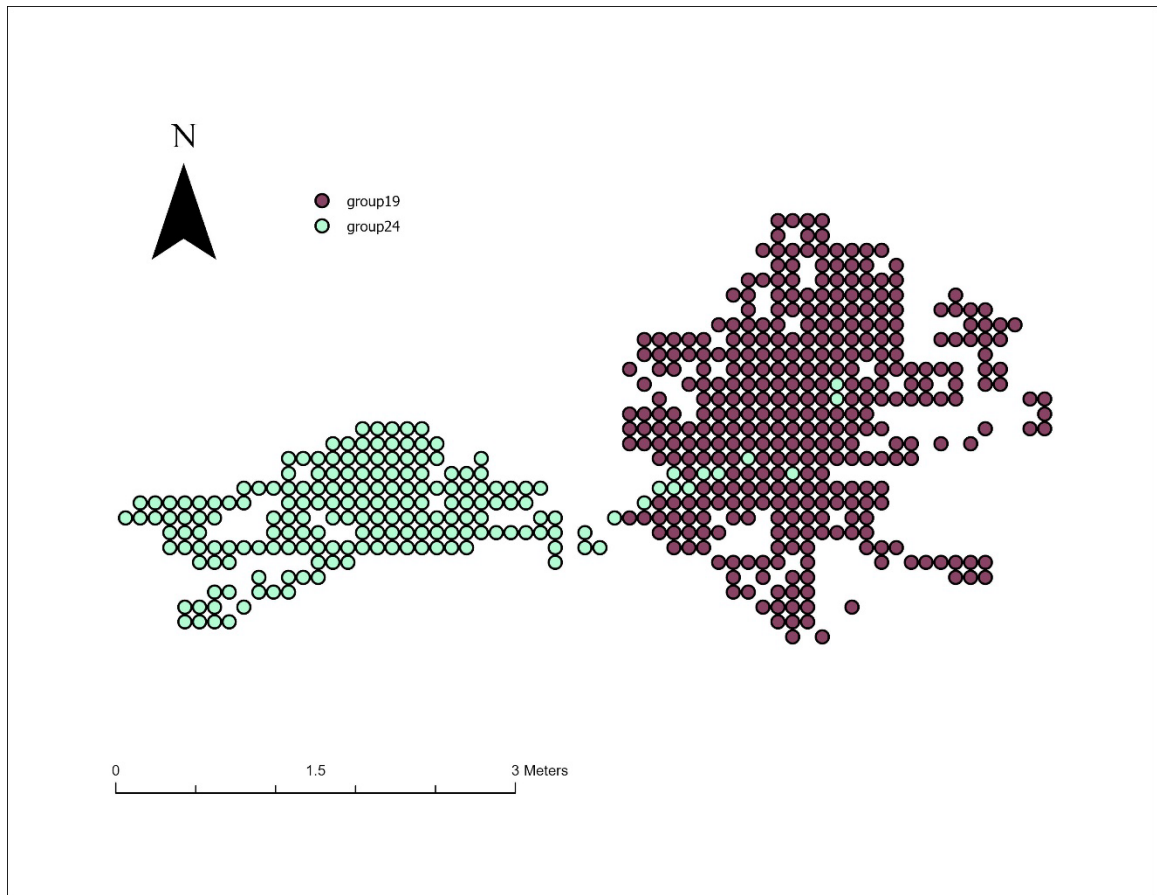


Figure 4.1 A 2D location map of data points from stationary tests group00019 and group00024 at Berea Road Soccer Complex, with no GPS post processing created by Alexandria Thomas.

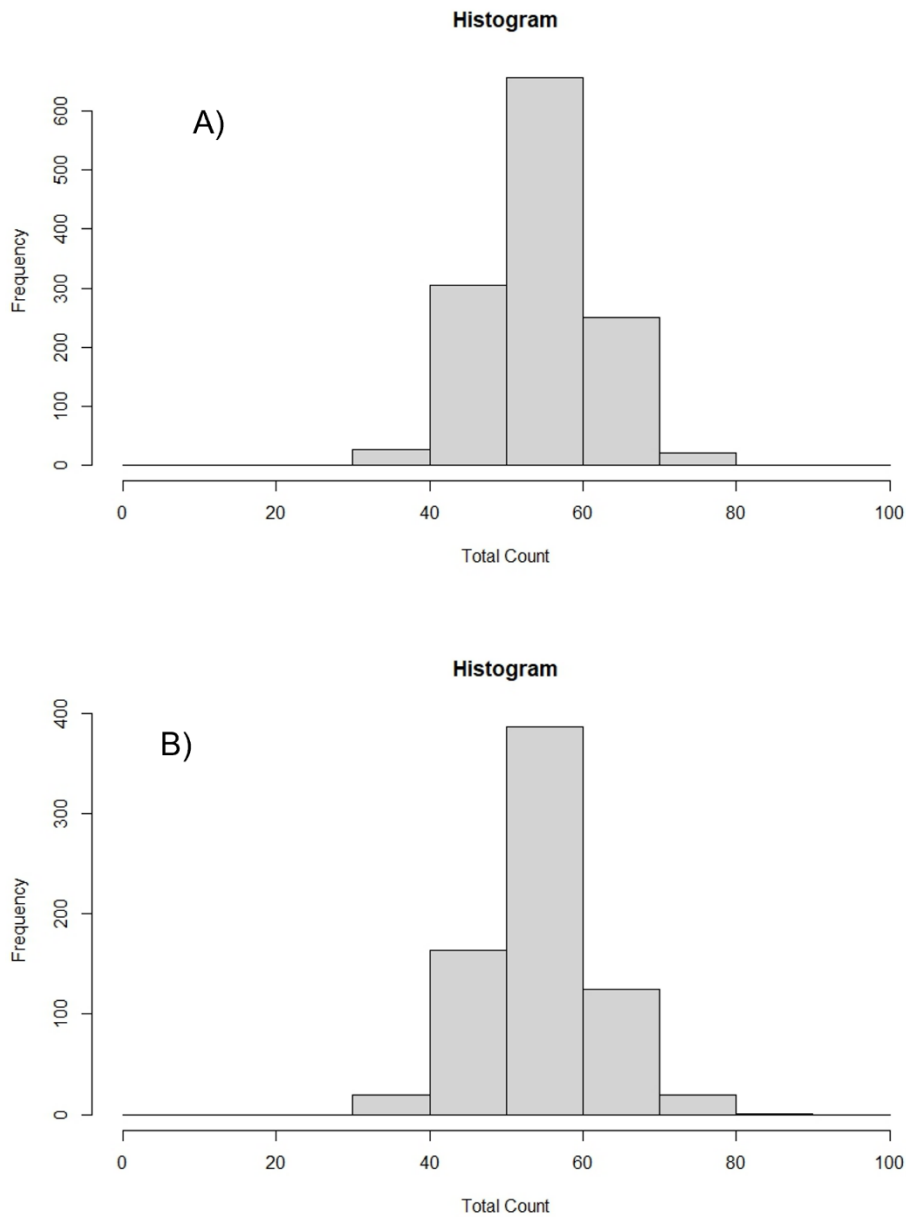


Figure 4.2 Groups 19 (A) and 24 (B) histograms were used to analyze the spectrometer variability of the UAV-mountable spectrometer.

#### 4.1.2 Spectrometer Variability – Stationary Test

To better understand the natural variability of the spectrometer receiver, redundant stationary ground tests were conducted. These tests were completed at location 1, location

4, and location 5. All the data shows an increase in total count measurements on soil compared to those taken on concrete or asphalt. Groups 15, 16 and 17 show consistent gamma measurements with a value difference of  $\pm 7$  for the minimum, 1st quartile, median, mean, 3rd quartile, and maximum and of  $\pm 0.1$  counts for the standard deviation (*Table 4.2*). The gamma measurements for Bluegrass soils of groups 19, 24, 25, 26, and 27 are consistent with a value difference of  $\pm 4$  for the minimum, 1st quartile, median, mean, 3rd quartile, and maximum and of  $\pm 1.1$  for the standard deviation (*Table 4.2*). The measurements are variable due to the low sensitivity of the detectors in the D230A, but the variability is repeatable at the same location.

Table 4.2 This shows the data statistics of all the stationary tests performed to analyze the effect of shielding, duration, surface type, and underlying geology on the instrument.

	Minimum (counts)	1 <sup>st</sup> Quartile (counts)	Median (counts)	Mean (counts)	3 <sup>rd</sup> Quartile (counts)	Maximum (counts)	Standard Deviation (counts)
<b>Stationary Ground</b>							
group 00015 (no shield)	26.00	48.00	53.00	53.18	58.00	79.00	7.134982
group 00016 (top shield)	33.00	48.00	53.00	53.11	58.00	76.00	7.003865
group 00017 (bottom shield)	28.00	41.00	46.00	45.82	51.00	68.00	6.729072
group 00019	32.00	50.00	55.00	55.00	60.00	78.00	7.130670
group 00024	34.00	50.00	55.00	55.09	60.00	83.00	7.399433
group 00025 (5m)	28.00	43.00	49.00	48.47	52.00	64.00	7.393245
group 00026 (5m)	32.00	43.00	48.00	47.90	52.25	67.00	6.201514
group 00027 (0m)	36.00	46.00	51.00	51.05	56.00	65.00	6.840141
<b>Duration Stationary - MMRB</b>							
group 34 – soil	21.00	32.00	36.00	36.08	40.00	59.00	6.054404

Table 4.2, continued.

group 35 – concrete	10.00	23.00	26.00	26.44	30.00	44.00	5.167982
group 36 – soil	17.00	32.00	36.00	36.01	40.00	58.00	6.013494
group 37 – concrete	12.00	23.00	26.00	26.26	30.00	44.00	5.210346
group 38 – soil	17.00	31.00	35.00	35.44	39.50	57.00	5.961438
group 39 – concrete	8.00	23.00	26.00	26.20	30.00	43.00	5.175583
group 40 – soil	15.00	31.00	35.00	35.37	39.00	61.00	6.058923
group 41 – concrete	9.00	22.00	26.00	25.94	29.00	46.00	5.073698
<b>Sinkhole</b>							
group 43 – soil	22.0000	36.0000	40.0000	40.4100	45.0000	56.0000	5.9392010

#### 4.1.3 Effects of Environment and Background

To evaluate possible atmospheric and background contributions, a stationary ground test was conducted with (a) no shielding, (b) shielding on top of the unit, and (c) shielding under the unit (*Figure 4.3*). A folded medical x-ray vest loaned by the Health Promotion Department in the University of Kentucky College of Education was used as a simple and easily available shield. All field tests were conducted in optimal weather conditions during the spring, summer, and fall of 2022 and winter of 2023 on days with clear skies and no precipitation conditions during the week of May 15th – 24th, 2022. Stationary and shielding tests were conducted at Location 1 outside of the Mining and Minerals Research Building on the University of Kentucky campus. At that location, stationary tests were shielded on the top, represented by group 00016 (*Figure 4.3b*) in the data catalog, and the bottom, represented by group 00017 (*Figure 4.3c*) in the data catalog, of the instrument using the x-ray vest. An un-shielded test, represented by group 00015 (*Figure 4.3a*), was performed immediately after the shielded tests. Shielding the spectrometer has no quantitative effect on the total counts collected. Histograms measuring

the total counts versus frequency were produced to show the statical change in the data. The statistical difference between the minimum, 1st quartile, median, mean, 3rd quartile, and maximum of each group is  $\pm 7$  and  $\pm 0.4$  between the standard deviation of each group (Table 4.3). All three histograms have a frequency range of 0 to 500 and a total count range of 0 to 100 (Figure 4.3) (Appendix).

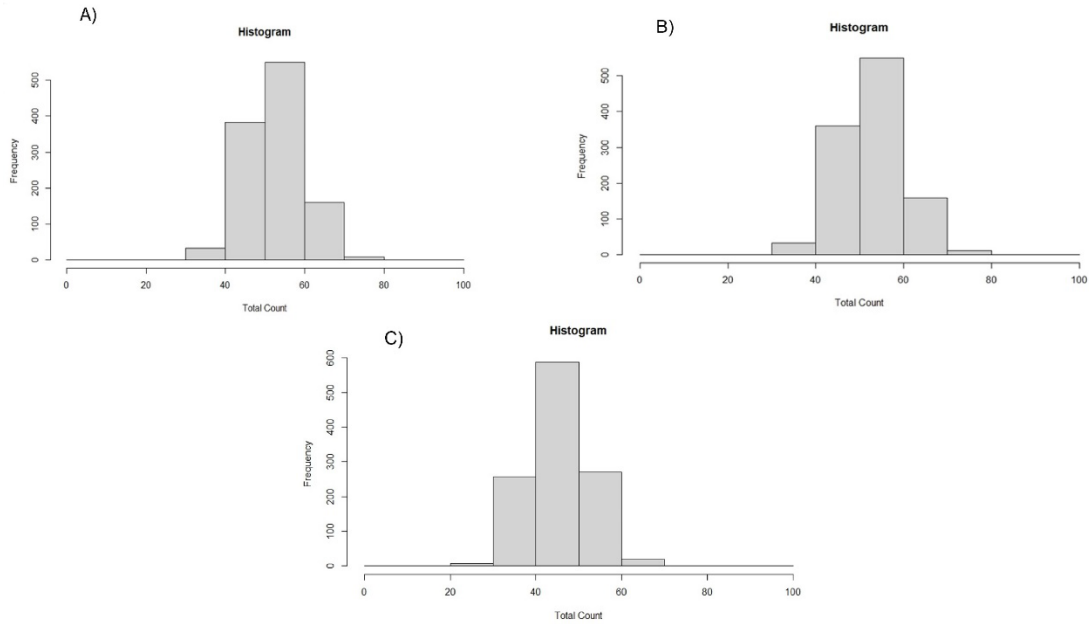


Figure 4.3 A diagram of the histograms from group 15 (A), 16 (B), and 17 (C) to show the effect of shielding to eliminate background contributions to the spectrometer.

Table 4.3 This table shows the data statistics of the effects of the study area environment and background using a shielding method on the instrument.

Stationary Ground	Minimum (counts)	1 <sup>st</sup> Quartile (counts)	Median (counts)	Mean (counts)	3 <sup>rd</sup> Quartile (counts)	Maximum (counts)	Standard Deviation (counts)
group 00015 (no shield)	26.00	48.00	53.00	53.18	58.00	79.00	7.134982
group 00016 (top shield)	33.00	48.00	53.00	53.11	58.00	76.00	7.003865
group 00017 (bottom shield)	28.00	41.00	46.00	45.82	51.00	68.00	6.729072



#### 4.1.4 Duration Variability – Stationary Test

To better understand the potential variability of the spectrometer, duration tests were conducted on soil, concrete, and asphalt outside of Location 1 (Mining and Minerals Resources Building) near a tree with exposed soil and a bike rack on concrete with minimal obstruction. The number of counts recorded, or frequency of points, increased with duration. Duration has no quantitative effect on the total count of the field area, meaning the total amount of records does increase with time for each sample collected on soil and asphalt, but the average frequency, or average number of counts, does not differ by a great amount. If approximately a thousand points are recognized on soil, then approximately a thousand points are recognized on asphalt. Therefore, the spectrometer is consistent with recognizing the lower total count in concrete and asphalt compared to soil. The data was collected for 4 durations of 5 minutes, 10 minutes, 20 minutes, and 1 hour each on both soil and concrete. A table and histograms were constructed to analyze the statistical data collected from the spectrometer (*Table 4.4; Figures 4.4 & 4.5*) (*Appendix*).

Soil groups, the groups of measurements only taken on soil material, numbered 34 (*Figure 4.4*), 36, 38, and 40 are statistically different by  $\pm 6$  counts for the minimum, 1st quartile, median, mean, 3rd quartile, and maximum of each group and  $\pm 0.9$  for the standard deviation of each group while the concrete groups 35 (*Figure 4.5*), 37, 39, and 41 are statistically different by  $\pm 4$  for the minimum, 1st quartile, median, mean, 3rd quartile, and maximum of each group and  $\pm 0.14$  for the standard deviation of each group (*Table 4.4*). Groups 34 and 35 have a frequency of points range of 0 to 150 and a total count range of 0 to 100 (*Figures 4.4 & 4.5*). The peak of group 34 ranges from 35 to 40 in total count at a

frequency of approximately 150 and the peak of group 35 ranges from 20 to 25 in total count at a frequency of approximately 150 (*Figures 4.4 & 4.5*).

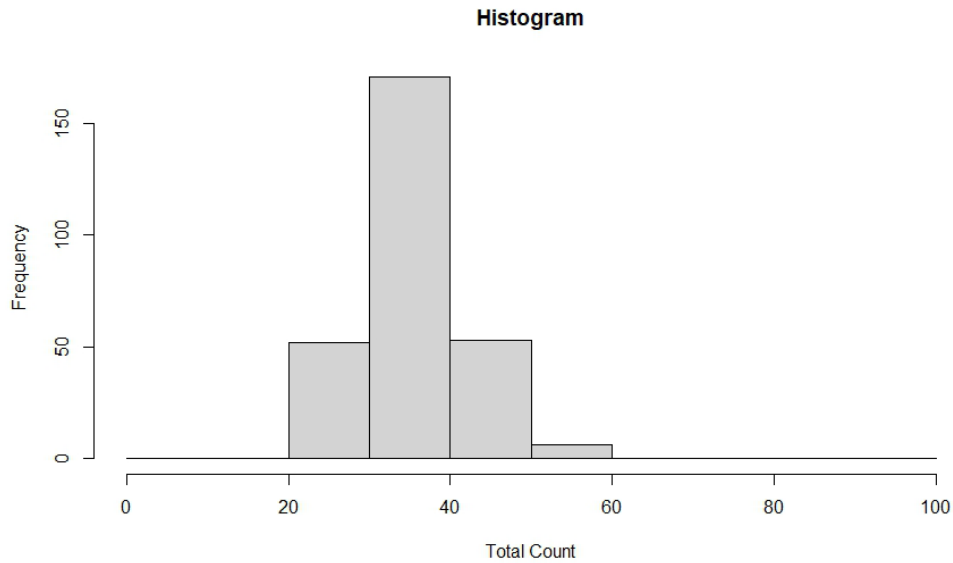


Figure 4.4 A histogram of group 34, a soil stationary test of the effect of duration.

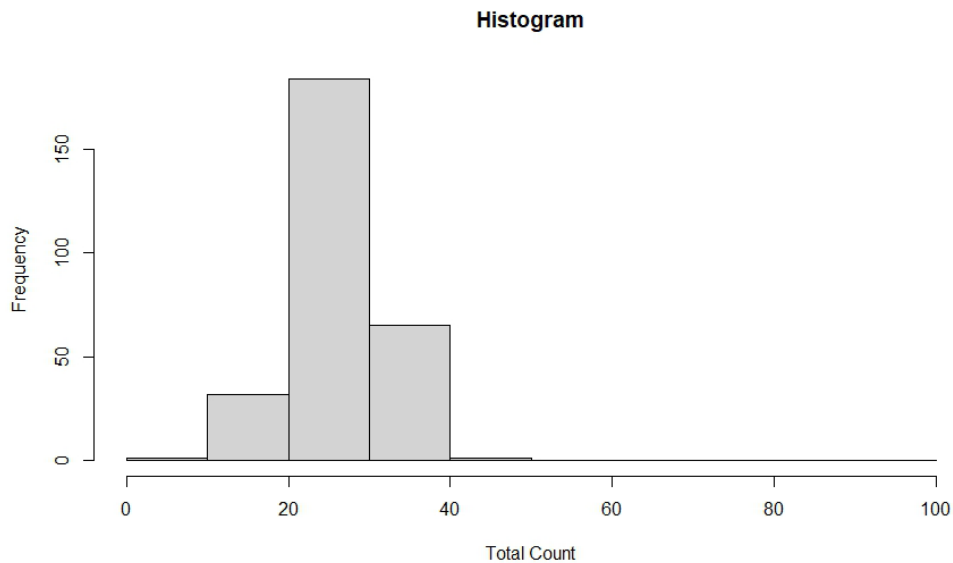


Figure 4.5 A histogram of group 35, a concrete stationary test of the effect of duration.

Table 4.4 A table of compiled data statistics from the duration tests.

Duration Stationary - MMRB	Minimum (counts)	1 <sup>st</sup> Quartile (counts)	Median (counts)	Mean (counts)	3 <sup>rd</sup> Quartile (counts)	Maximum (counts)	Standard Deviation (counts)
group 34	21.00	32.00	36.00	36.08	40.00	59.00	6.054404
group 35	10.00	23.00	26.00	26.44	30.00	44.00	5.167982
group 36	17.00	32.00	36.00	36.01	40.00	58.00	6.013494
group 37	12.00	23.00	26.00	26.26	30.00	44.00	5.210346
group 38	17.00	31.00	35.00	35.44	39.50	57.00	5.961438
group 39	8.00	23.00	26.00	26.20	30.00	43.00	5.175583
group 40	15.00	31.00	35.00	35.37	39.00	61.00	6.058923
group 41	9.00	22.00	26.00	25.94	29.00	46.00	5.073698

#### 4.1.5 Effect of Height Above the Ground – Vertical Test

Vertical flight tests were conducted with the UAV to determine the impact of altitude on the total counts recorded. Total counts decreased with altitude; however, care must be taken to recognize averaging from adjacent materials of varying gamma contribution. Vertical profiles were conducted at Location 2, 3, and 4 (Jacobson Park, World and Berea Road Soccer Complex) in Lexington, Kentucky. The data shows that the total count number fluctuates but decreases as elevation increases (*Figure 4.6*). The graphs also show that there are points at which the count number fluctuates (*Figure 4.7*). As height above ground increases, the total count decreases linearly within the range of elevation. Scatter plots were produced in RStudio from the tables created in MakeD (*Appendix*). The scatterplot is an elevation ranging over 25 m (260 ft to 340ft in elevation on the scatterplot) versus a total count ranging from 0 to 70 with Group00004 (A) being higher in elevation than Group00032 (B) (*Figure 4.7*). The statistical difference is  $\pm 4$  for the minimum, 1st quartile, median, mean, 3rd quartile, and maximum of each group and  $\pm 0.4$  for the standard deviation of each group (*Table 4.5*).

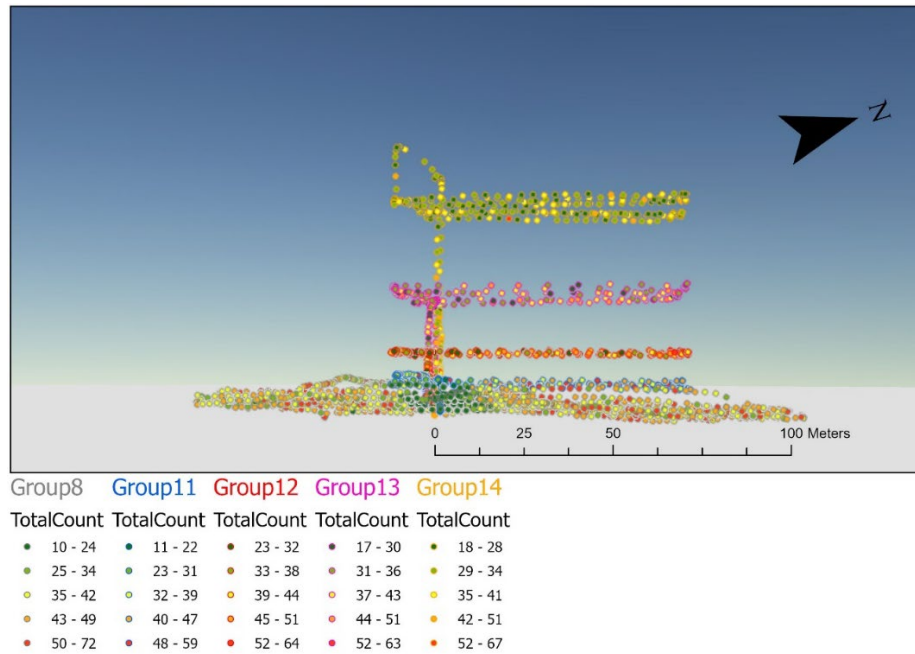


Figure 4.6 A 3D map of the change in height for each flight path of groups 8, 11, 12, 13, and 14 at Location 2.

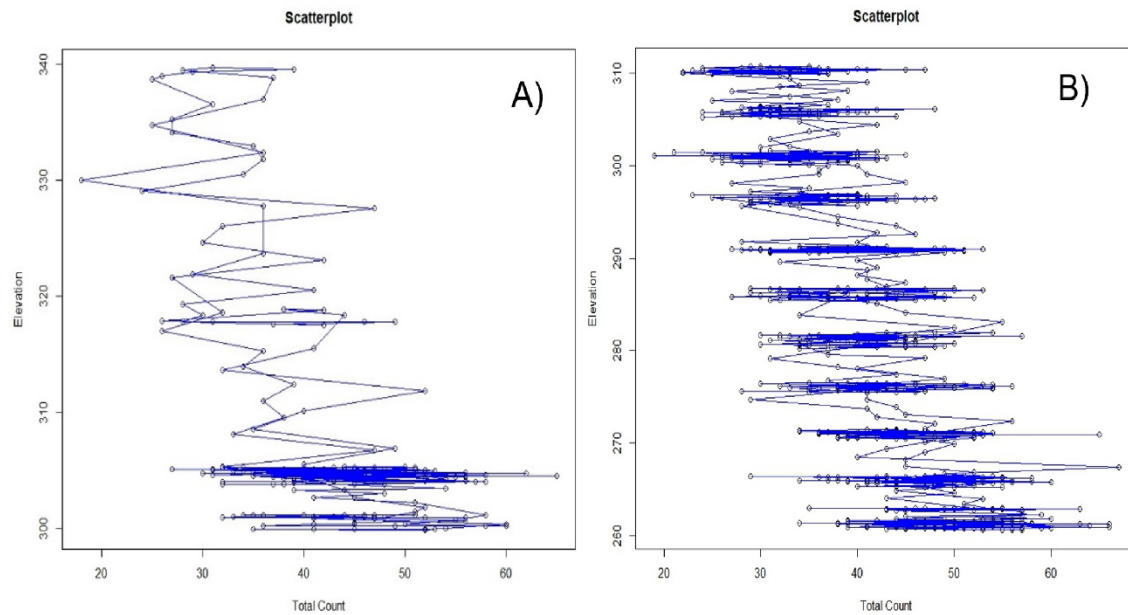


Figure 4.7 Scatterplots of group 4 (A) and group 32 (B) evaluate the effect of height above the ground showing an increase in total count as elevation decreases.

Table 4.5 A table of data statistics from the vertical stack test flights conducted to evaluate the effect of height above the ground.

Vertical Stack	Minimum	1 <sup>st</sup> Quartile	Median	Mean	3 <sup>rd</sup> Quartile	Maximum	Standard Deviation
group 4 soil	18.00	36.25	42.00	42.15	47.00	65.00	8.230042
group 00031 soil	22.00	36.75	42.00	42.35	47.25	64.00	7.979442
group 00032 soil	19.00	35.00	40.00	40.86	46.75	67.00	8.371822
group 00033 soil	23.00	35.00	39.00	39.59	44.00	63.00	6.527385

#### 4.1.6 Replicability

Two walking grids of a small footprint were conducted at Location 4 (Berea Road Soccer Complex). One grid was walked by Dr. William “Drew” Andrews at a 1.2-meter height while I conducted the other was conducted by me at a one-meter height, both following the same grid pattern. The data collected from Berea Road Soccer Complex following an identical profile is consistent considering the insignificant change in height above ground and time elapsed. Results from two walking profiles in which the spectrometer was carried by hand demonstrate the repeatability of the data obtained from the unit. Group 22 (A) has a frequency range of 0 to 300 and a total count range of 0 to 100 with a peak ranging from 30-40 total count (*Figure 4.8*). Group 23 (B) has a frequency range of 0 to 400 and a total count range of 0 to 100 with a peak ranging from 30 to 40 (*Figure 4.8*). There are few value differences with this data set as the minimum and maximum have the most difference of  $\pm 8$  and  $\pm 5$ . The standard deviation differs by  $\pm 0.2$  (*Table 4.6*).

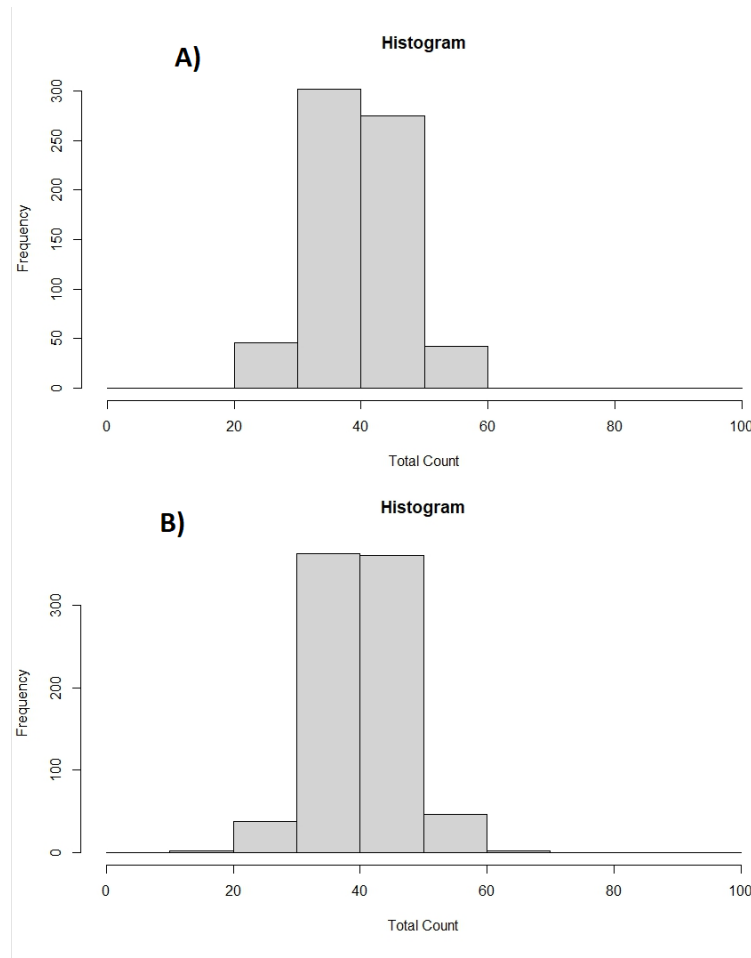


Figure 4.8 Histograms from group 22 (A) and group 23 (B) to evaluate the replicability of the instrument data collection.

Table 4.6 A table of data statistics from the walking surveys for replicability tests.

Walking Survey	Minimum (counts)	1 <sup>st</sup> Quartile (counts)	Median (counts)	Mean (counts)	3 <sup>rd</sup> Quartile (counts)	Maximum (counts)	Standard Deviation (counts)
(A) group 00022	25.00	36.00	40.00	40.18	45.00	59.00	6.316734
(B) group 00023	17.00	36.00	41.00	40.72	45.00	64.00	6.534739

#### 4.1.7 Recognizing Different Materials

Using multiple walking surveys, varying ground cover types such as soil, concrete, and asphalt showed variability in spectrometer results. Stacked, the same profile performed more than once, walking profiles were conducted at 1.2m altitude in a two-phase soil-

asphalt area at Location 2 (World Games Way), in northern Lexington, Kentucky. The soil values showed a mean of 43.8 total counts, and the asphalt shows a mean of 17.5 total counts. The profiles illustrate the internal variability of materials inferred to be internally consistent and illustrate the contrast between the two varied materials. This data can also be used to infer that the footprint of observation is approximately three times the altitude of measurement above the ground surface. Stacked multi-altitude profiles at 1.2 m, 5 m, and 10 m across a two-phase soil-asphalt profile at World Games Way were conducted as well. The spatial footprint of observation increases with altitude, producing a decreased resolution of transitions between each material with increasing altitude. In general, the measurements of total counts decrease with increased height above the ground due to the reduction of the amplitude of radiation particles with the increase in height. The spectrometer can differentiate boundaries between materials at 1-meter and 10-meter heights, and that data is represented in the point data visualization in ArcGIS Pro. When comparing the statistics of the soil to the statistics of the asphalt for two-phase material analysis, the asphalt values are between 22.01 and 37.00 for the mean (*Figure 4.9*), while the soil values are between 34.30 and 42.84 for the mean (*Figure 4.10*). For three-phase material analysis, comparison of the mean values for asphalt at 20.66, for concrete ranging from 31.42 to 34.90, and for soil ranging from 42.36 to 43.40. The standard deviation for soil ranges approximately 7.3 to 8.2 and for asphalt ranges approximately 4.5 to 7.4 of the two-phase material analysis opposed to three-material analysis of asphalt at approximately 6.9 of concrete from approximately 6.7 to 8, and of soil from approximately 6.8 to 7.1 (*Table 4.7*). The mean value takes into consideration the total count number versus the frequency of points resulting in a lower value in asphalt than in soil.

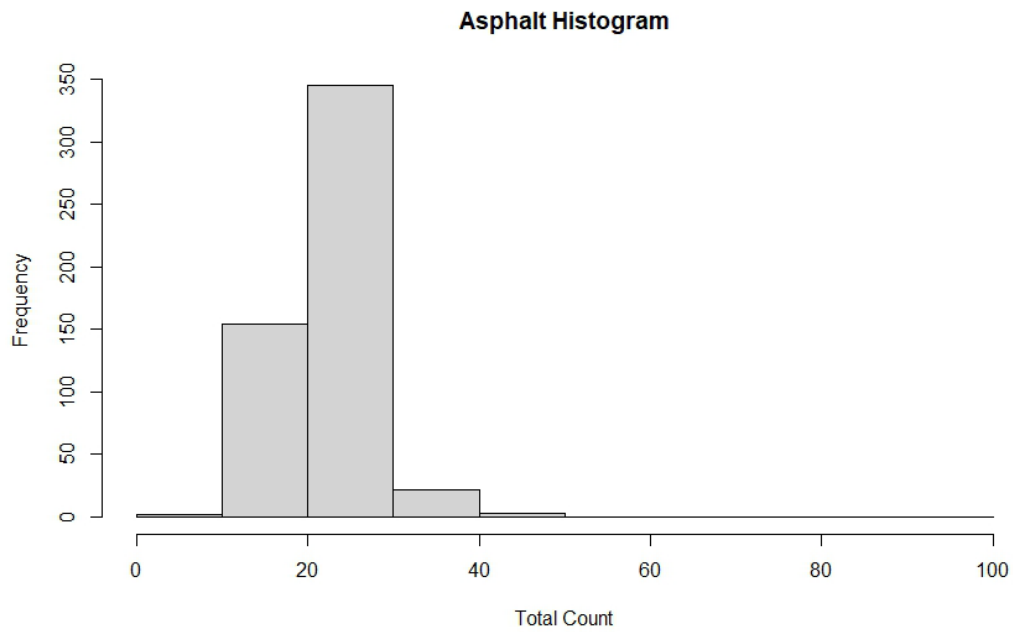


Figure 4.9 Group 8 asphalt histogram showing a lower total count statistic range.

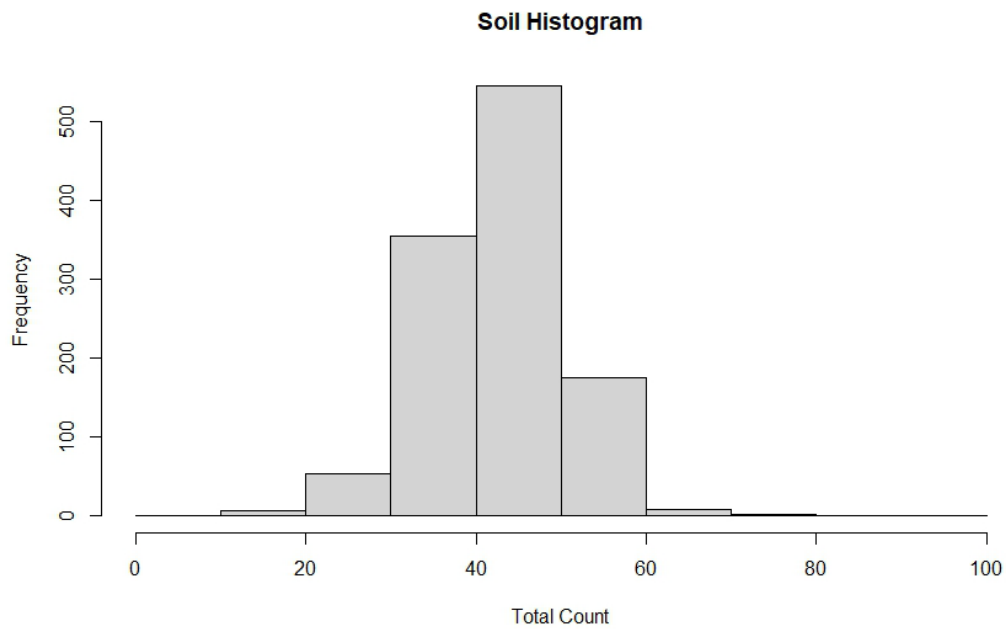


Figure 4.10 Group 8 soil histogram showing a higher count statistic range.



Table 4.7 Survey data statistics of tests over different materials with known and visible transitions.

<b>WGW Two phase</b>	<b>Minimum (counts)</b>	<b>1<sup>st</sup> Quartile (counts)</b>	<b>Median (counts)</b>	<b>Mean (counts)</b>	<b>3<sup>rd</sup> Quartile (counts)</b>	<b>Maximum (counts)</b>	<b>Standard Deviation (counts)</b>
group 8 soil	12.00	38.00	43.00	42.84	48.00	72.00	7.600777
group 8 asphalt	10.00	18.00	23.00	22.01	23.00	45.00	4.519462
group 11 soil	20.00	36.00	41.00	41.86	48.00	59.00	7.989742
group 11 asphalt	11.00	22.00	27.00	26.85	32.00	49.00	7.434040
group 12 soil	24.00	36.00	41.00	41.45	47.00	64.00	7.375696
group 12 asphalt	23.00	29.50	33.00	33.78	37.00	51.00	6.750119
group 13 soil	17.00	34.00	38.00	38.72	43.00	63.00	7.515406
group 13 asphalt	24.00	33.00	34.00	34.62	37.00	45.00	4.708095
group 14 soil	18.00	29.00	33.00	34.30	38.00	67.00	7.950309
group 14 asphalt	21.00	27.00	32.00	31.64	34.00	44.00	4.879684
<b>Jacobson Park Two- phase</b>							
group 4 soil	18.00	36.25	42.00	42.15	47.00	65.00	8.230042
group 5 asphalt	10.00	19.00	22.00	22.77	26.75	39.00	5.395821
group 5 soil	21.00	36.00	41.00	41.36	46.00	71.00	7.828188
group 6 asphalt	15.00	23.00	25.00	25.92	29.00	40.00	5.387108
group 6 soil	18.00	32.00	37.00	37.18	42.00	60.00	7.617690
group 7 asphalt	8.00	15.00	19.00	19.80	23.75	37.00	5.684128
group 7 soil	25.00	37.00	41.00	41.36	45.00	64.00	6.290129
<b>MMRB Three- Phase</b>							
group 3 soil	22.00	37.00	42.00	42.36	47.00	65.00	7.127038
group 3 asphalt	7.00	16.00	20.00	20.66	24.00	45.00	6.852566
group 3 concrete	13.00	29.00	35.00	34.90	40.00	62.00	7.998926
group 18 soil	27.00	38.00	43.00	43.40	48.00	63.00	6.750550
group 18 concrete	13.00	26.25	32.00	31.42	36.00	43.00	6.730070

#### 4.1.8 Footprint

To better understand the footprint and visibility of measurements with altitude, a methodical vertical profile was measured with the UAV-compatible spectrometer at 1 m, 5 m, 10 m, 20 m, and 40 m. The resulting profile shows the spatial distribution of average counts per second of the transition from the soil with a high average to the asphalt with a low average. As height above ground increases, the size of the average footprint covered by the spectrometer increases as well. Based on the statistical data, the soil means ranges from 37.18 to 42.15 while the asphalt ranges from 19.80 to 25.95. The standard deviation between soil ranges from 7.8 to 8.2 and between asphalt ranges from approximately 5.4 to 5.7 (*Table 4.8*). According to the footprint, soil averages range from 159.3 counts per second at ground level to 121.67 counts per sec 2-meters above ground level while asphalt averages range from 114.67 counts per second at ground level to eighty-four counts per second at 2-meters above ground level (*Figure 4.11*).

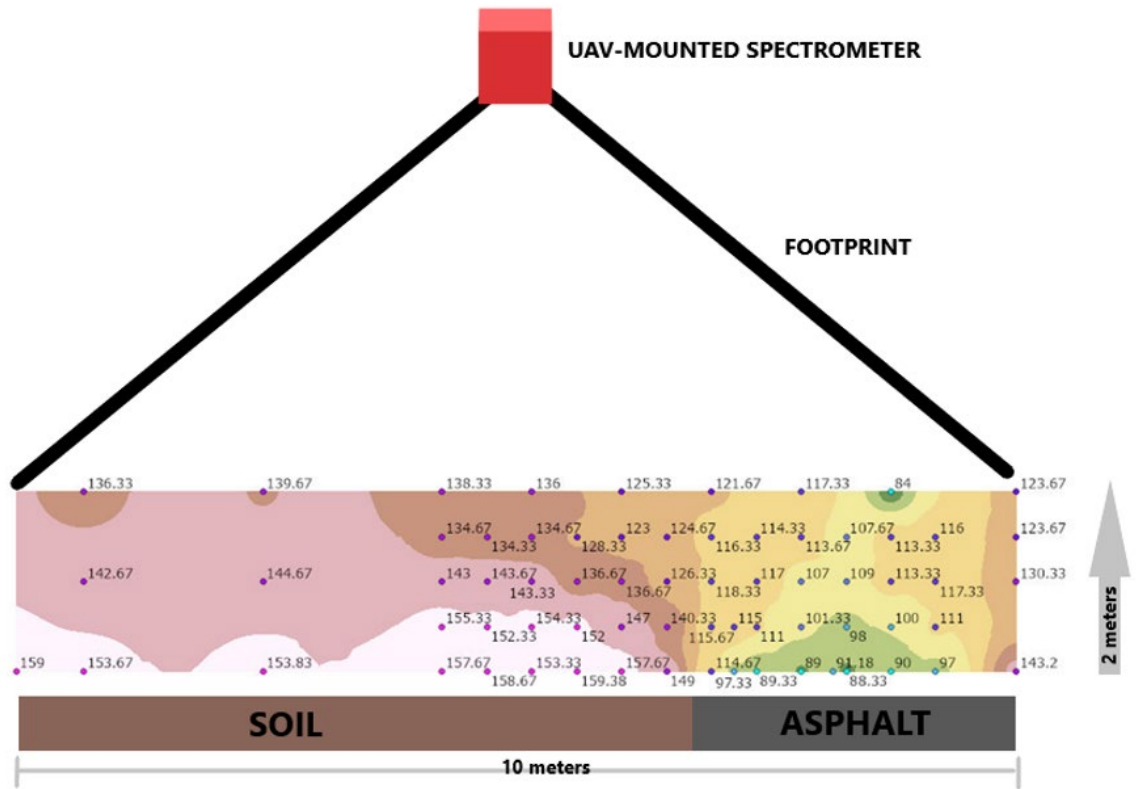


Figure 4.11 Sketch of the footprint produced by the spectrometer while 2 meters above ground level.

Table 4.8 Data statistics used to analyze the footprint of the instrument over asphalt and soil.

Jacobson Park Two-phase	Height (m)	Minimum (counts)	1 <sup>st</sup> Quartile (counts)	Median (counts)	Mean (counts)	3 <sup>rd</sup> Quartile (counts)	Maximum (counts)	Standard Deviation (counts)
group soil 4	5-40	18.00	36.25	42.00	42.15	47.00	65.00	8.230042
group asphalt 5	5	10.00	19.00	22.00	22.77	26.75	39.00	5.395821
group soil 5	5	21.00	36.00	41.00	41.36	46.00	71.00	7.828188
group asphalt 6	20	15.00	23.00	25.00	25.92	29.00	40.00	5.387108
group soil 6	20	18.00	32.00	37.00	37.18	42.00	60.00	7.617690
group asphalt 7	1.2	8.00	15.00	19.00	19.80	23.75	37.00	5.684128

Table 4.8, continued.

group 7 soil	1.2	25.00	37.00	41.00	41.36	45.00	64.00	6.290129
--------------	-----	-------	-------	-------	-------	-------	-------	----------

#### 4.1.9 Topographic Effect of a Sinkhole

To evaluate the effect of topography on the emission of count particles detected by the spectrometer, walking surveys over a sinkhole were conducted. Field tests were conducted at Location 5 (Hardin County) outside of Fort Knox. At a walking pace, three groups were created to cover the area of each sinkhole. The statistical data from these groups did not show any significant information from the counts collected with the spectrometer to show that there might have been a topographic effect. The mean and standard deviation reflect a similar count value as the previous test done to understand the parameters of the instrument at a mean value of approximately forty counts and a standard deviation value of approximately 6 counts. A map was produced in ArcGIS Pro to visualize the topographic effect of the sinkhole on the data from the spectrometer (*Figure 4.12*). The data demonstrates most of the points located in the low points of the sinkhole. A graph of average distance using the UTM (Universal Transverse Mercator) coordinates of the data collected from the spectrometer verses average total count was created in ArcGIS Pro to demonstrate most of the counts accumulated within the first 15 m of the surveyed area (*Figure 4.14*). The table below shows the average total count statistics from groups 42, 43, and 44 both within and outside of the sinkhole profile (*Table 4.9*). While there is a higher frequency of points within the sinkhole (*Figure 4.12*), the frequency, or number of times a total count occurs, differs +/- 0.85 in the mean value. There is a higher number of total counts of photons within the sinkhole, and a higher number of times a total count of photons

occurs outside of the sinkhole. A lidar map was created to have a better representation of the sinkhole and the space the points were collected in (*Figure 4.13*).

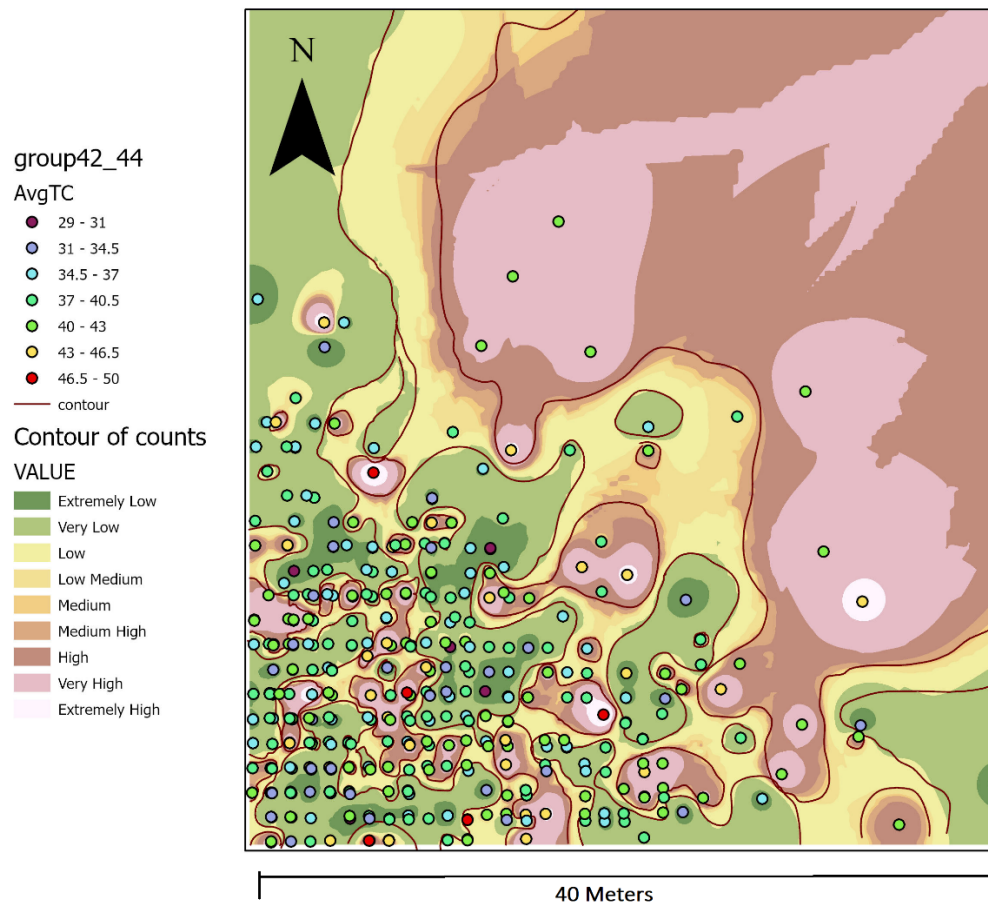


Figure 4.12 Contour map of the sinkhole data produced from the spectrometer.

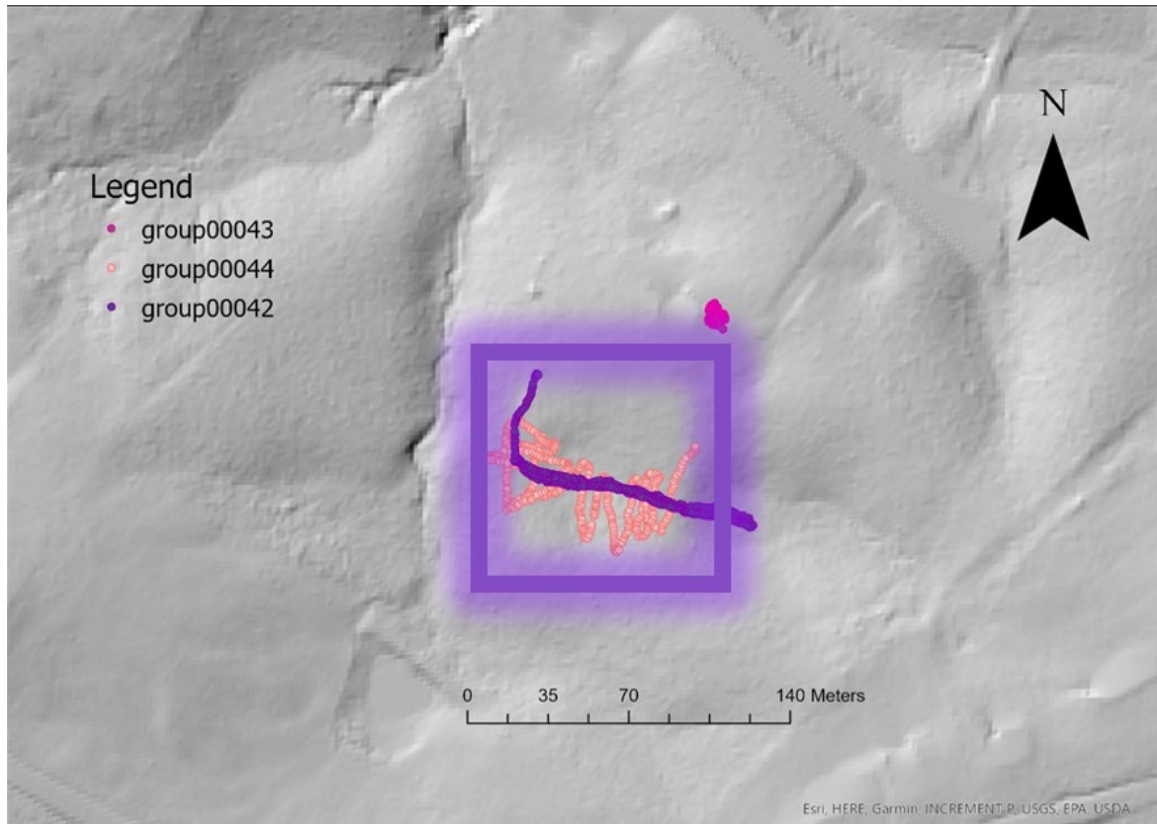


Figure 4.13 A lidar map of the area where the sinkhole is at location 5 produced in ArcGIS Pro from data source from the online catalog of a 5-foot digital model with hillshade effect applied. The purple square indicates the points covered in on the contour map in Figure 4.12.

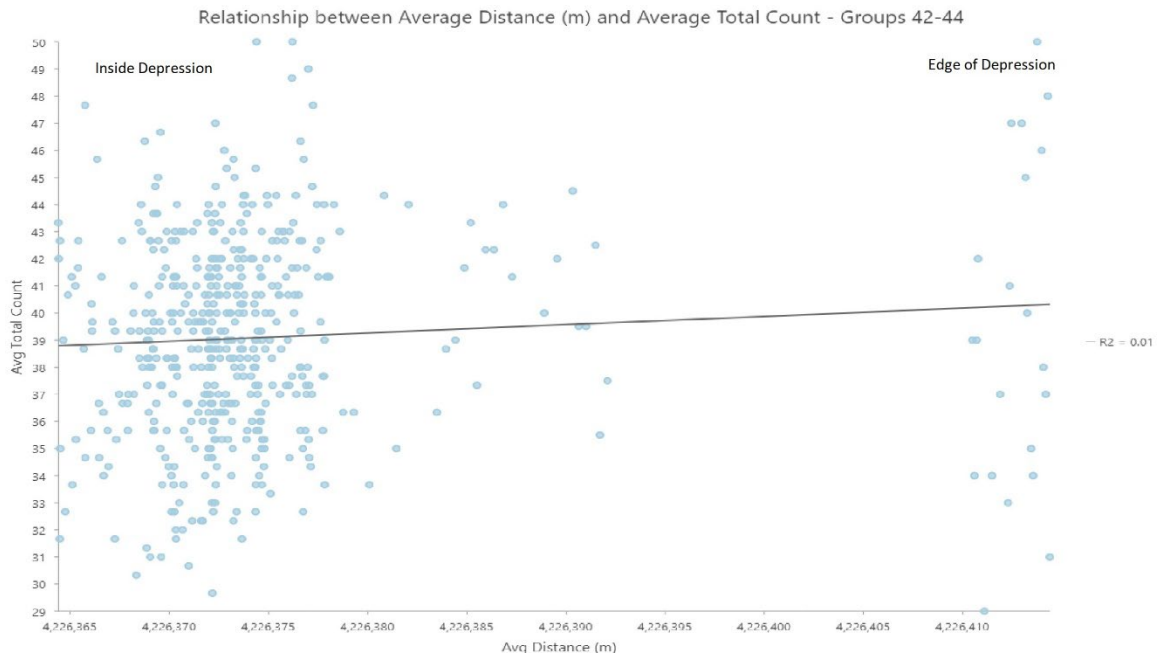


Figure 4.14 Average distance verses average total count of groups 42 through 44 that were conducted over an area with a sinkhole.

Table 4.9 The data statistics used to analyze the effect of topography.

Sinkhole	Minimum (counts)	1st Quarter (counts)	Median (counts)	Mean (counts)	3rd Quarter (counts)	Maximum (counts)	Standard Deviation (counts)
Average of groups 42-44 (outside)	32.6700	37.0000	40.3300	39.8700	42.3300	45.6700	3.3864070
Average of groups 42-44 (within)	29.0000	36.5000	39.0000	39.0200	41.5000	50.0000	3.7018520

#### 4.1.10 Fault Transect

To evaluate the effect of faults on total counts detected by the spectrometer, walking surveys over two parallel faults were conducted. The next set of tests were completed at Location 6 (Alumni Drive). At a walking pace, two transects were completed across three different stratigraphic units separated by two faults. The units were Clays Ferry Formation containing shale, limestone, and siltstone; Garrard Siltstone containing siltstone

and limestone; and Tanglewood Limestone Member No. 2 containing limestone and shale. Most of the point data have a high total count value in the Garrard Siltstone formation. There is also evidence of a spike in total count near the division where the faults occur. Plots analyzing the moving mean and moving standard deviation were produced to understand the effect of stratigraphic units and fault positions to the data. The data shows a linear fluctuation of data with small spikes at the location of the faults and major spikes between 300 and 650 meters (*Figure 4.15*). This data compared to the average distance verses average total count scatterplot show many of the total counts overlap with the Garrard Siltstone unit (*Figure 4.16*). According to the table, the mean of the total count is 50.8200 with a standard deviation of approximately 9.7, a uranium mean value of 0.8800, and a uranium standard deviation of approximately 0.94 (*Table 4.10*).



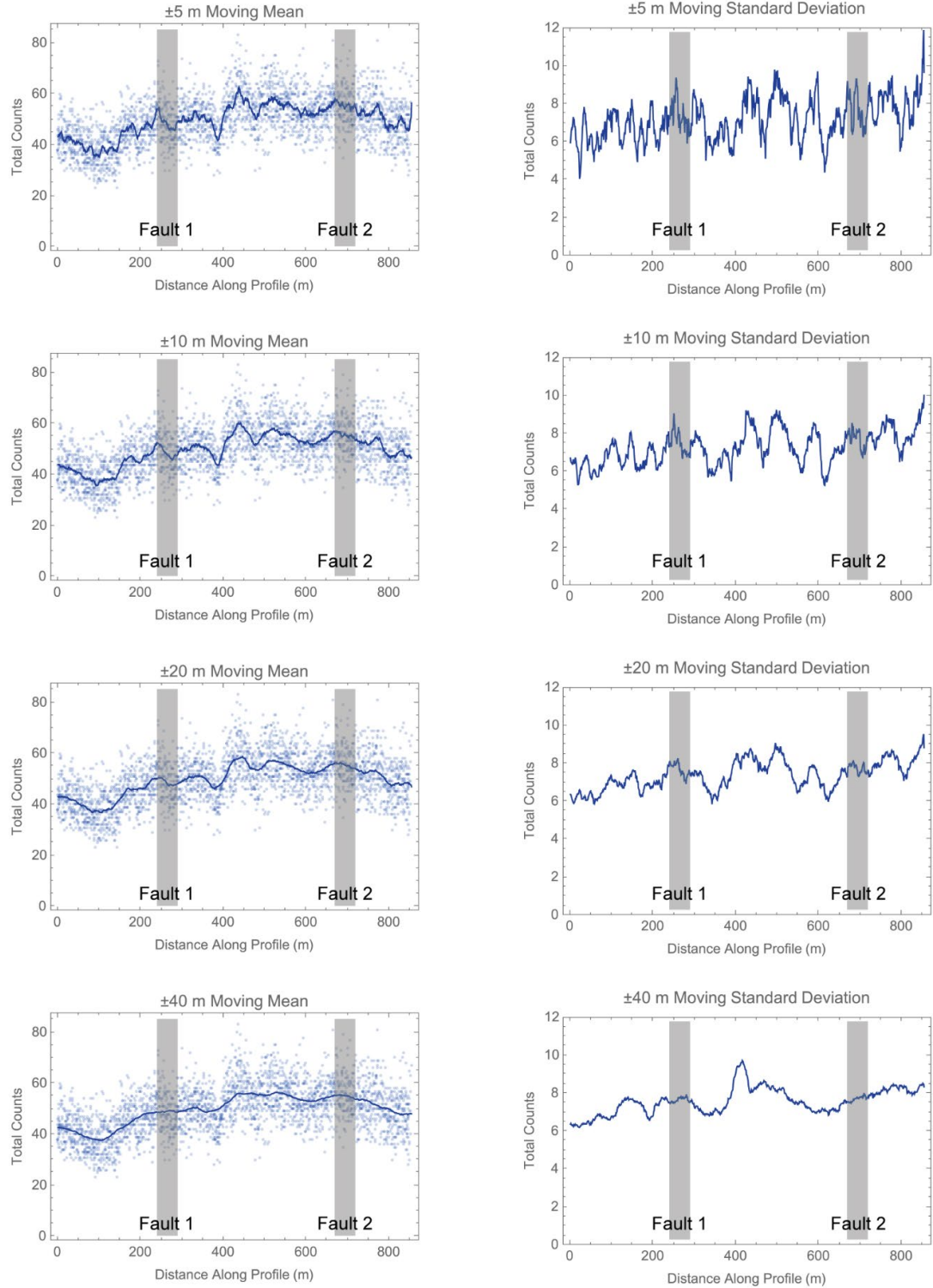


Figure 4.15 A plot of the total counts (blue), moving mean (blue line with light blue points), and moving standard deviation (dashed blue line) using a  $\pm 5\text{m}$ ,  $\pm 10\text{m}$ ,  $\pm 20\text{m}$ , and  $\pm 40\text{m}$  window along the fault profile with the western end to the left.

Table 4.10 The data statistics from the fault transect with a known transition to understand its effect on the instrument.

<b>Fault/sinkhole</b>	<b>Minimum (counts)</b>	<b>1st Quartile (counts)</b>	<b>Median (counts)</b>	<b>Mean (counts)</b>	<b>3rd Quartile (counts)</b>	<b>Maximum (counts)</b>	<b>Standard Deviation (counts)</b>
group 45 Total count	23.0000	44.0000	51.0000	50.8200	57.0000	83.0000	9.6584960
group 45 uranium	0.0000	0.0000	1.0000	0.8800	1.0000	6.0000	0.9367940
group 45 Thorium	0.0000	0.0000	0.0000	0.6053	1.0000	4.0000	0.7478888
group 45 Potassium	0.0000	2.0000	4.0000	4.0990	5.0000	15.0000	2.2177610

## CHAPTER 5. DISCUSSION

Each test gave an essential result which was used to infer if the UAV-compatible spectrometer is efficient for radionuclide mapping. Stationary tests to understand the GPS reliability of the instrument showed an offset of roughly  $\pm 2$  m with nearly identical statistic values from the total count data which leads to the interpretation that the GPS is highly reliable because the data varies very little or not at all. Stationary tests to understand the spectrometer variability over multiple media and locations showed statistical data of little variation with produced histograms of a bell curve ranging from 30-90 total counts in the domain and a peak mean between 50-60 total counts. This result means the spectrometer's behavior when measuring photons is consistent at a control state. Two shielded stationary tests and one unshielded stationary test were conducted to understand how the surrounding environment may influence the instrument. These show that the shielding that is currently most compatible with the payload of the instrument is not significant enough to affect the background measurements from the environment. This is reflected by the bell curve between the total count domain of 20-80 and peaking mean between 40 and 60 total counts with each histogram of groups 15, 16, and 17. With this result, we decided shielding was not applicable to this instrument with the resources available. Duration stationary tests were conducted to understand the effect of time on the total count measured by the instrument. Results show an increase in records collected as time increases, with a lower mean total count in asphalt and concrete than in soils. We expected this result of the test because we know the values are lower in asphalt and concrete has a similar composition to asphalt. The increased amount of time allows the machine to collect more points as it runs. Therefore,

duration does not appear to affect the overall mean total count of both soil and asphalt. After conducting vertical test flights to determine the effect of height above the ground at locations 2, 3, and 4, results show a decrease in the average total count value as height above the ground increases. We inferred that this is due to the dissipation of the uranium, thorium, and potassium isotope photons, and due to the increased footprint of the instrument. Replicability was tested by creating two nearly identical grids of data resulting in nearly identical calculated statistics. Based on the results from each test, we confirmed the accuracy and precision of the instrument and led the team to conclude that the spectrometer could successfully produce photon data with little to no error. Surveys conducted over multiple surface materials of soils, asphalt and/or concretes helped determine the machine's ability to recognize different surface materials. Our team conducted surveys over multiple surface materials including soils, asphalts, concretes, and bedrocks and our results show a change in the average total count for each material. Similarly, surveys that measure transitions from asphalt to concrete show a continued decrease in the average total count. We inferred that asphalt and concrete act as blocking agents for the emission of isotope photons from the soil or underlying bedrock. Two-phase vertical profiles were conducted to understand the footprint and visibility of the instrument resulting in an increased footprint and visibility with the increase in height above the ground. These increases are due to the functionality of the instrument which allows photons to be recorded only when there are limited or no obstructions in the view of the machine. With an increased height above ground level, the footprint of the spectrometer increases, and the total photon count is decreased, resulting in a decrease in the overall resolution of the instrument. This decrease in resolution also affects the recognition of different surface

materials showing an imprecise gradient of differentiated materials. Two tests were done to understand the potential to determine signatures of geologic features. The first test was a survey over a sinkhole at approximately 1-m height. Results show a higher total photon count within the sinkhole potentially due to a greater amount of emission of isotope photons being released from the sinkhole. The second test was a fault transect over two mapped parallel faults separating three stratigraphic units resulting in an increase in total count over the Garrard Siltstone. We inferred that this unit has a greater emission due to its composition and its overlying soil composition being affected by redistribution.

The range of variation of the instrument is much greater than the range of variation of the geologic and climatic environment. The instrument varies between an average total photon counts of 19.80 and 55.09 counts. As for the range of variation of the geologic environments, each surface material in the data sequence offers a different range of average total count. Asphalt ranges from a total count average of 19.80 to 34.62 counts, concrete ranges from an average of 31.42 to 34.90 counts, soil ranges from an average of 25.94 to 55.09 counts, sinkholes range from an average of 35.68 to 41.13 counts, and three stratigraphic units separated by faults range from an average of 48.45 to 50.82 counts. Since the tests conducted for this project span a two-year period, the climate varies across all seasonal changes. Overall, the seasonal variations ranged in temperatures as low as 19 degrees and as high as 84.9 degrees Fahrenheit, excluding days with heavy precipitation and snow coverage.

Limitations of the lightweight spectrometer and UAV unit discovered during this project place important constraints on its potential to collect data for radon potential mapping. Because of the weight threshold the UAV must maintain to have a successful

flight pattern, our attempts at shielding using an x-ray vest to block the background emissions were not feasible, since the most effective shielding would add to the payload of the spectrometer. Given the limitations of the lightweight spectrometer and UAV, they are efficient for producing low-level radiometric data collections, so long as tests are conducted at a maximum height of ten meters above ground level for optimal conditions to be achieved. The height verses sensitivity relationship means that flying heights would be very low, maybe too low to make UAV-borne gamma spectrometers impractical for radon potential mapping.

Our results suggest optimal conditions and fieldwork strategies to increase the reliability of the instrument. Fieldwork considerations are 1) grid plans of ten meters or less above the ground at 2 m/s speed, 2) multiple surface or subsurface materials, 3) lack of obstructions, 4) and warm, dry climate. These were chosen because the height and speed of the survey impacts the footprint, surface type impacts the average total count, obstructions impact the limit on the path and grid size, and weather impacts the functionality of the instrument and the rate of emission from the surface material.

The scope of this project was limited to measuring a photon count rather than a complete radioactive atom and the data generated is not adequate for comprehensive radionuclide soil mapping. In future work, it may be useful to incorporate a comparison of the photon average measurements to the average radionuclide values from soil samples or other surface materials from each test site. Our ability to measure the complete isotope was limited by the expense of radioactive isotope analysis and the time required to collect and analyze radioactive material. Additionally, understanding the calibration factors required to relate soil radionuclide quantities to gamma production and the attenuation factors for

different source distances is a challenge. These are all important thoughts and considerations for the work that may extend from my project.

The prevalence of karst in Kentucky, and the complex relationship between karst and radon mapping point toward the need for future research in this area. Specifically, because they exhibit some sort of fracture or ventilation in the earth allowing the broken rock to accumulate and exhale the elevated levels of uranium/radon concentrations into the atmosphere. A spectrometer is more likely to pick up elevated readings over known areas of fracture or ventilation, which karst exhibits.

Overall, these preliminary data suggest that the gamma measurements for Bluegrass soils are consistent. The measurements are relatively variable due to the low sensitivity of the detectors in the D230a, but the variability is repeatable at the same location. The data collected over time from one location is replicable but shows significant internal variability in the data recorded. We refrained from further attempts to shield the spectrometer, as it would require a thicker, more restraining shield that would increase the payload of the instrument and make it unattainable to conduct flights with the UAV system. There was a minimal impact from the background if the environment was unchanged. Current results from the two-phase profile suggest this small UAV-compatible spectrometer is a useful near-surface reconnaissance tool for identifying significant soil variation. Careful data-collection planning and awareness of the local environmental conditions are essential. Lower height-above-ground and slower-velocity flight plans are preferred for more practical data results. There is also evidence in the tests at Location 6 of a spike in total count near the division where the faults occur indicating the sensitivity of the spectrometer

is strong enough to detect the increase in the potential risk of uranium exposure in lithologies and near faults.



## CHAPTER 6. CONCLUSION

Radon is the second leading cause of lung cancer in the United States, and the World Health Organization has launched an international radon project to increase awareness, collect data, encourage prevention, and inspire other scientists to investigate prevention solutions to this problem. Since radon exposure and underlying geologic conditions are direct correlations to each other, awareness and prevention work are imperative, and new radionuclide mapping methods with UAV-compatible spectrometers are key to improving this work. The results generated by our field tests confirmed our hypothesis that radionuclide levels over different surfaces (soil, asphalt, rock type, faults, sinkholes, and karsts) will differ enough to be interpreted as separate ground types and signatures of geologic features could be detected by the lightweight, UAV-compatible spectrometer. Specifically, our tests of GPS reliability, spectrometer footprint, effect of height, sinkhole analysis, and transect over a known fault and bedrock transition prove the hypothesis of this work to be true and therefore prove the accuracy and precision of the instrument to be for future radionuclide mapping at low levels for high resolution. This project was proven to be useful for the potential use for soil radionuclide mapping based on the data above. It is important to understand that while the overall experiment was successful, the machine has the potential to improve in data collection and processing with time and method collaboration. The success of this project helps fill the research gap to contribute to measuring and mapping radionuclide data. More broadly, this project's work on radon mapping contributes to ongoing work at the University of Kentucky around radon exposure and mitigation in the state. There are interesting lines of research related to

lithologic, stratigraphic, and structural geologic controls on radon levels in Kentucky, and this work and more future work done by others contribute to understanding radon mobility in near-surface formations.

## APPENDICES

Commands for producing a histogram in RStudio (1). Commands for producing statistical data in RStudio to construct a table (2). Commands for producing a scatterplot with a logarithmic regression line in RStudio (3). Workflow for creating a visual representation of the point data in ArcGIS Pro (4).

## APPENDIX 1. PRODUCE A HISTOGRAM

Enter commands as follows:

```
> distn <- read.csv("R:/Working_Data/GeoRadisD230Adata/groupXXXXXX/x.csv")  
> summary(distn$TotalCount)  
> hist(distn$TotalCount, main = "Histogram", xlab = "Total Count", breaks = c(0, 10, 20,  
30, 40, 50, 60, 70, 80, 90, 100))
```

## APPENDIX 2. PRODUCE A STATISTICAL ANALYSIS

Enter commands as follows:

```
> distn <- read.csv("R:/Working_Data/GeoRadisD230Adata/groupXXXXXX/x.csv")  
  
> summary(distn$TotalCount)  
  
> sd(distn$TotalCount)
```

### APPENDIX 3. PRODUCE A SCATTERPLOT AND LOGARITHMIC REGRESSION

#### LINE

Enter commands as follows:

```
> distn <-  
read.csv('Y:/Working_Data/GeoRadisD230Adata/group00032/BereaRdAUGv8_EDITED.csv')  
  
> plot(distn$TotalCount, distn$Altitude, main = "Scatterplot", xlab = "Total Count", ylab = "Elevation")  
  
> model <- lm(distn$Altitude ~ log(distn$TotalCount))  
  
> summary(model)  
  
> x = seq(from=0, to=100, length.out=1000)  
  
> y = predict(model, newdata = list(x=seq(from=0, to=80, length.out=1000)), interval = "confidence")  
  
> matlines(distn$TotalCount, distn$Altitude, col = "blue")
```

#### APPENDIX 4. ARCGIS PRO WORKFLOW

1. Import csv file to ArcGIS Pro.
2. Convert to point data.
  - a. Right click table > display XY data > X, Y, and Z set to Long, Lat, and Altitude
3. Change base map to imagery.
4. Add polygon feature class > draw polygon around point data > following the boundaries of the asphalt and soil.
5. Click analysis > Tools > spatial Join > select target feature as point data > select join feature as polygon data > name output feature class > Select join operation 'join on to many' > match option 'intersect'> RUN
6. Export spatial join table
  - a. Open attribute table of spatial join data > click the three bars 'MENU' in the upper right-hand corner of the attributes window > export > name output table and include .csv

## REFERENCES

- Al-Zoughool, M., & Krewski, D. (2009). Health effects of radon: A review of the literature. *International Journal of Radiation Biology*, 85, 57-69. <https://doi.org/10.1080/09553000802635054>
- Anderson, W. H., Sparks, T. N., & Weisenfluh, G. A. (2004). Completion of the first phase of the Kentucky digital geologic mapping program. In *Digital mapping techniques '04—Workshop proceedings* (U.S. Geological Survey Open-File Report 2004–1451). Washington, DC: U.S. Geological Survey. Retrieved from <https://pubs.usgs.gov/of/2004/1451/anderson/index.html>
- Aydar, E., and Diker, C., 2021, Carcinogen soil radon enrichment in a geothermal area: Case of Güzelçamlı-Davutlar District of Aydın City, Western Turkey: *Ecotoxicology and Environmental Safety*, v. 208, p. 111466, doi: 10.1016/j.ecoenv.2020.111466.
- Ball, T. K., and Miles, J. C. H. (1993). Geological and geochemical factors affecting the radon concentration in homes in Cornwall and Devon, UK. *Environ. Geochem. Health* 15(1), 27-36.
- Barron, A.R., 2011, *Radioactive Decay Series: General Chemistry*, [http://www.vias.org/genchem/nuclear\\_chem\\_31328\\_04\\_04.html](http://www.vias.org/genchem/nuclear_chem_31328_04_04.html) (accessed March 2023).
- Baykara, O., İnçeöz, M., Doğru, M., Aksoy, E., and Kuşlahcı, F.: Soil radon monitoring and anomalies in East Anatolian Fault System (Turkey), *J. Radioanal. Nucl. Ch.*, 279(1), 159–164, doi:10.1007/s10967-007-7211-2, 2009.
- Beck, H L., Condon, W.J., Lowder, W. M., 1964. *Spectrometric Techniques for Measuring Environmental Gamma Radiation*. Health and Safety Laboratory New York Operations Office, AEC New York, New York, 71 p. - Available on: [http://digital.library.unt.edu/ark:/67531/metadc13094/m2/1/high\\_res\\_d/HASL-150.pdf](http://digital.library.unt.edu/ark:/67531/metadc13094/m2/1/high_res_d/HASL-150.pdf) (accessed: 03.01.2017).
- Beck, H. L., De Campo, J., Gogolak, C., 1972. *In Situ Ge(Li) and Na(Tl) Gamma-Ray Spectrometry*. Scientific Report, HASL-258. Environmental Measurements Laboratory, U.S. Atomic Energy Commission. New York, 86 p. - Available on: <https://www.osti.gov/scitech/servlets/purl/4599415/> (accessed: 03.01.2017).
- Black, D. F. B., Cressman, E. R., and MacQuown, W. C., Jr., 1965, *The Lexington Limestone (Middle Ordovician) of central Kentucky*: U.S. Geol. Survey Bull. 1224-C, 29 p.
- Campbell, M. R., 1898, *Description of the Richmond quadrangle, Kentucky*: U.S. Geol. Survey Geol. Atlas, Folio 46.
- Centers for Disease Control and Prevention. *Extinguishing the tobacco epidemic in Kentucky*: United States Department of Health and Human Services; 2018.



<https://www.cdc.gov/tobacco/about/osh/program-funding/pdfs/kentucky-2018-508.pdf>. Accessed 21 Aug 2018.

Chiavacci, S. J., Shapiro, C. D., Pindilli, E. J., Casey, C. F., Rayens, M. K., Wiggins, A. T., et al. (2020). Economic valuation of health benefits from using geologic data to communicate radon risk potential. *Environmental Health*, 19, 1–9. <https://doi.org/10.1186/s12940-020-00589-8>

Committee on Health Risks of Exposure to Radon. Biological Effects of Ionizing Radiation VI (BEIR VI), National Research Council. Health effects of exposure to indoor radon. Washington, D.C: The National Academies Press; 1999.

Cressman, E. R. (1973). Lithostratigraphy and depositional environments of the Lexington Limestone (Ordovician) of central Kentucky. (Professional Paper 768). Washington, DC: U.S. Geological Survey.

Cressman, E. R., & Noger, M. C. (1981). Geologic mapping of Kentucky; a history and evaluation of the Kentucky Geological Survey-U.S. Geological Survey Mapping Program, 1960-1978 (Circular 801). Washington, DC: U.S. Geological Survey.

Currens, J. C. (2002). Kentucky is karst country! What you should know about sinkholes and springs. (Information Circular 4, Series 12). Lexington, KY: Kentucky Geological Survey.

D230A v2 UAV Gamma-Ray Spectrometer, 2020, Georadis s.r.o. - Instruments for Detection of Radiation, <http://www.georadis.com/en/products/d230a.html> (accessed February 2023).

Danilchik, Walter, and Hyden, H. J., 1956, Midcontinent Pennsylvanian rocks, in Geologic investigations for radioactive deposits, semiannual progress report, Dec. 1, 1955, to May 31, 1956: U.S. Geol. Survey TEL-620, p. 259-261, issued by U.S. Atomic Energy Comm. Tech. Inf. Service, Oak Ridge, Tenn.

Day, W.C., Drenth, B.J., McCafferty, A.E., Shah, A.K., Ponce, D.A., Jones, J.V., III, and Grauch, V.J.S., 2019, The U.S. Geological Survey's Earth Mapping Resources Initiative (Earth MRI)— Providing framework geologic, geophysical, and elevation data for the Nation's critical mineral bearing regions: *Fast times*, v. 24, p. 55–61.

De Meijer, R.J., Limburg, J., Venema, L.B., 2002. Natural radioactivity in monitoring waste disposals. *Phys. Scr.* T97, 139–147.

Duval, J. S., Carson, J. M., Holman, P. B., & Darnley, A. G. (1993). Terrestrial radioactivity and gamma-ray exposure in the United States and Canada (Open-File Report 2005–1413). Washington, DC: U.S. Geological Survey.

Duval, J. S., Cook, B., and Adams, J. A. S., 1971, A study of the circle of investigation of an airborne gamma-ray spectrometer: *Journal of Geophysical Research*, v. 76, p. 8466-8470.

- EPA, Health Risk of Radon, 2023, <http://www.epa.gov/radon/health-risk-radon> (accessed February 2023).
- Fogh, C.L., Andersson, K.G., Barkovsky, A.N., et al., 1999. Decontamination in a Russian settlement. *Health Phys.*, Vol. 76, No. 4, pp. 421–430.
- Gillmore, G.K., Crockett, R.G., and Przylibski, T.A., 2010, Preface "IGCP Project 571: Radon, health and natural Hazards": *Natural Hazards and Earth System Sciences*, v. 10, p. 2051–2054, Doi: 10.5194/nhess-10-2051-2010.
- Grasty, R. L. and Darnley, A. G., 1971, Calibration of gamma-ray spectrometers for ground and airborne use: Geological Survey of Canada Paper 71-17, 27p.
- Green, B. M. R., Lomas, P. R., and O'Riordan, M. C. (1992). Radon in Dwellings in England. *Natl. Radiol. Protect. Board Rep.* R254.
- Groves-Kirkby, C. J., Denman, A. R., Phillips, P. S., Crockett, R. G. M., and Sinclair, J. M.: Comparison of seasonal variability in European domestic radon measurements, *Nat. Hazards Earth Syst. Sci.*, 10, 565–569, doi:10.5194/nhess-10-565-2010, 2010.
- Hahn EJ. Smoke-free Ordinance Database. Lexington: Kentucky Center for Smoke-free Policy; 2019. [www.breathe.uky.edu](http://www.breathe.uky.edu). Accessed 11 July 2019.
- Hahn, E. J., Gokun, Y., Andrews, W. M. Jr., Overfield, B. L., Robertson, H., Wiggins, A., & Rayens, M. K. (2015). Radon potential, geologic formations, and lung cancer risk. *Preventive Medicine Reports*, 2, 342–346. <https://doi.org/10.1016/j.pmedr.2015.04.009>
- Haneberg, W. C., Wiggins, A., Curl, D. C., Greb, S. F., Andrews, W. M., Rademacher, K., et al. (2020). A geologically based indoor-radon potential map of Kentucky. *GeoHealth*, 4, e2020GH000263. <https://doi.org/10.1029/2020GH000263>
- Hyland, R., and Gunn, J. (1994). International comparison of cave radon concentrations identifying the potential alpha radiation risks to British cave users. *Health Physics* 67, 76}179.
- Irwin, D. J., and Knibbs, A. J. (1977). *Mendip; Underground: A Cavers Guide*. Mendip, Somerset.
- Inan, S., Akgul, T., Seyis, C., Saatçılar, R., Baykut, S., Ergintav, S., and Bas, M.: Geochemical monitoring in the Marmara region (NW Turkey): A search for precursors of seismic activity, *J. Geophys. Res.*, 113, B03401, doi:10.1029/2007JB005206, 2008.
- Karathanasis, A. D. (1991). Phosphate mineralogy and equilibria in two Kentucky Alfisols derived from Ordovician limestones. *Soil Science Society of America Journal*, 55(6), 1774–1782. <https://doi.org/10.2136/sssaj1991.03615995005500060045x>
- Kentucky Geological Survey Interactive Geologic Map., 2020, [kgs.uky.edu](http://kgs.uky.edu), <https://kgs.uky.edu/kygeode/geomap/?gkarst=true> (accessed March 2023).

Khan, H. A., Tufail, M., and Qureshi, A. A.: Radon signals for earthquake prediction and geological prospection, *J. Islamic Academy of Sciences*, 3(3), 229–231, 1990.

Koomans, R.L., Limburg, J., 2005. In situ mapping of heavy metal concentrations and organic micro compounds. In: *Proceedings of the Third International Conference on Remediation of Contaminated Sediments*, Venice, 2005. Batelle Press, Columbus, USA.

Lagarde, F., Axelsson, G., Damberg, L., Mellander, H., Nyberg, F., & Pershagen, G. (2001). Residential radon and lung cancer among never-smokers in Sweden. *Epidemiology*, 12(4), 396–404. <https://doi.org/10.1097/00001648-200107000-00009>

Lantz, P.M., Mendez, D., Philbert, M.A., 2013. Radon, smoking, and lung cancer: the need to refocus radon control policy. *Am. J. Public Health* 103, 443–447.

Lexington-Fayette Climate, Weather By Month, Average Temperature (Kentucky, United States), 2023, Weather Spark, <https://weatherspark.com/y/15790/Average-Weather-in-Lexington-Fayette-Kentucky-United-States-Year-Round#Figures-Temperature> (accessed March 2023).

Mahajan, S., Walia, V., Bajwa, B. S., Kumar, A., Singh, S., Seth, N., Dhar, S., Gill, G. S., and Yang, T. F.: Soil gas radon/helium surveys in some neotectonic areas of NW Himalayan foothills, India, *Nat. Hazards Earth Syst. Sci.*, 10, 1221–1227, doi:10.5194/nhess-10-1221-2010, 2010.

Martin et al., 2016 P.G. Martin, O.D. Payton, J.S. Fardoulis, D.A. Richards, Y. Yamashiki, T.B. Scott Low altitude unmanned aerial vehicle for characterizing remediation effectiveness following the FDNPP accident *J. Environ. Radioact.*, 151 (2016), 10.1016/j.jenvrad.2015.09.007

Matrice 600 - DJI, 2016, DJI Official, <http://www.dji.com/matrice600> (accessed February 2023).

McDowell, R. C. (1986). *The geology of Kentucky; A text to accompany the geologic map of Kentucky* (Professional Paper 1151-H). Washington, DC: U.S. Geological Survey.

McFarlan, A. C. (1943). *Geology of Kentucky*. Lexington, KY: University of Kentucky.

McFarlan, A.C., 1943, Blue Grass, in *Geology of Kentucky*, Lexington, Kentucky, University of Kentucky.

Medeiros, F.H.M., Yoshimura, E.M., 2005. Influence of soil and buildings on outdoor gamma dose rates in Sao Paulo, Brazil. *Health Phys.*, Vol. 88, No. 1, pp. 65–70.

Medusa Radiometrics BV, 2020 Medusa Radiometrics BV <http://medusa-radiometrics.com> (2020) accessed 12.9.19.

Mendez, D., Alshanqueety, O., Warner, K. E., Lantz, P. M., & Courant, P. N. (2011). The impact of declining smoking on radon-related lung cancer in the United States. *American Journal of Public Health*, 101(2), 310–314. <https://doi.org/10.2105/AJPH.2009.189225>

- Miles, J. C. H., Green, B. M. R., and Lomas, P. R. (1992). Radon affected areas: Derbyshire, Northamptonshire, and Somerset. *Documents Natl. Radiol. Protect. Bd.* 3(4), 19}28.
- Moore, G. W., 1954, Extraction of uranium from aqueous solution by coal and some other materials: *Econ. Geology*, v. 49, no. 6, p. 652-658.
- Muikku M, Heikkinen T, Puhakainen M, Rahola T, Salonen L. 2007. Assessment of occupational exposure to uranium by indirect methods needs information on natural background variations. *Radiation Protection Dosimetry* 125:492-495.
- Mwalongo, D.A., Haneklaus, N.H., Lisuma, J.B., Kivevele, T.T., and Mtei, K.M., 2022, Uranium in phosphate rocks and mineral fertilizers applied to agricultural soils in East Africa: *Environmental Science and Pollution Research*, v. 30, p. 33898–33906, doi: 10.1007/s11356-022-24574-5.
- Nam HS, Ryu JS. Indoor radon and lung cancer: national radon action plans are urgently required. *Yonsei Med J.* 2018;59(9):1013–4.
- Nicolet, J.P., Erdi-Krausz, G. Guidelines for Radioelement Mapping Using Gamma Ray Spectrometry Data vol. 179, International Atomic Energy Agency (2003) [http://www-pub.iaea.org/MTCD/publications/PDF/te\\_1363\\_web.pdf](http://www-pub.iaea.org/MTCD/publications/PDF/te_1363_web.pdf)
- Otton, J.K., 1992, The Geology of Radon: U.S. Department of the Interior/ U.S. Geological Survey, doi: 10.3133/7000018.
- Overfield, B. L., Andrews, W. M., Robertson, H., Rayens, M. K., & Hahn, E. J. (2016). Radon research collaboration between the Kentucky Geological Survey and the University of Kentucky College of Nursing: An innovative partnership. In *Special Papers* (Vol. 520, pp. 267–271). Boulder, CO: Geological Society of America. [https://doi.org/10.1130/2016.2520\(23\)](https://doi.org/10.1130/2016.2520(23))
- Peacock, J. D., and Taylor, K. (1966). Uraniferous collophane in the Carboniferous limestone of Derbyshire and Yorkshire. *Bull. Geol. Surv. Great Britain* 25, 19}32.
- Phillips, P. (1995). A remarkable story. In *The Radon Manual, Second Edition: A Guide to the Requirements for the Detection and Measurement of Natural Radon Levels. Associated Remedial Measures and Subsequent Monitoring of Results*, pp. 1.1}1.36. Radon Council Ltd., Shepperton, Middlesex.
- Pirkle, F.L., Pirkle, W.A., and Rich, F.J., 2013, Heavy-mineral mining in the Atlantic Coastal Plain and what deposit locations tell us about ancient shorelines: *Journal of Coastal Research*, v. 69, p. 154–175, [https://doi.org/10.2112/SI\\_69\\_11](https://doi.org/10.2112/SI_69_11).
- Planinic, J., Radolic, V., and Culo, D.: Searching for an earthquake pre-cursor: temporal variations of radon in soil and water, *Fizika B*, 9(2), 75–82, 2000.
- Radionuclide Basics: Radon, 2022, EPA, <http://www.epa.gov/radiation/radionuclide-basics-radon> (accessed February 2023).

Radon and Cancer, 2022, Does Radon Cause Cancer? | American Cancer Society, <http://www.cancer.org/healthy/cancer-causes/radiation-exposure/radon.html> (accessed February 2023).

Ramzaev, V., Barkovsky, A., Bernhardsson, C., Mattsson, S. Calibration and testing of a portable NaI(Tl) gamma-ray spectrometer-dosimeter for evaluation of terrestrial radionuclides and <sup>137</sup> Cs contributions to ambient dose equivalent rate outdoors. *Radiatsionnaya Gygiena = Radiation Hygiene*, 2017, Vol. 10, No. 1, pp. 18-29. DOI: 10.21514/1998-426x-2017-10-1-18-29

Ramzaev, V., Barkovsky, A., 2015. On the relationship between ambient dose equivalent and absorbed dose in air in the case of large-scale contamination of the environment by radioactive cesium. *Radiatsionnaya Gygiena. Radiation Hygiene*, Vol. 8, No. 3, pp. 21–32. -Available on: <http://www.radhyg.ru/jour/article/view/242/260> (accessed: 03.01.2017).

Ramzaev, V., Yonehara, H., Hille, R., et al., 2006. Gamma-dose rates from terrestrial and Chernobyl radionuclides inside and outside settlements in the Bryansk Region, Russia in 1996–2003. *J. Environ. Radioact.*, Vol. 85, No. 2–3, pp. 205–227.

Reimann, C., Filzmoser, P., 1999. Normal and lognormal data distribution in geochemistry: death of a myth. Consequences for the statistical treatment of geochemical and environmental data. *Environ. Geol.* 39, 1001–1914.

Rozhkova, E. V., Basumnaya, E. G., Serebryakova, M. B., and Shcherbak, O. V., 1958, The role of sorption in the process of uranium concentration in sedimentary rocks: Second Internat. Conf. on Peaceful Uses of Atomic Energy Proc., Geneva, 1958, v. 2, p. 420-431.

Roy, P.S., 1999, Heavy mineral beach placers in southeastern Australia: Their nature and genesis: *Economic Geology and the Bulletin of the Society of Economic Geologists*, v. 94, p. 567-588, <https://doi.org/10.2113/gsecongeo.94.4.567>.

Shah, A., Morrow, R., Pace, M., Harris, M., and Doar, W., 2021, Mapping Critical Minerals from the Sky: *GSA Today*, v. 31, p. 4–10, doi: 10.1130/gsatg512a.1.

SPH Engineering, 2023, UgCS expert monthly subscription: UgCS, <https://shop.ugcs.com/products/ugcs-expert-monthly-subscription> (accessed March 2023).

Sundal, A.V., Henriksen, H., Soldal, O., Strand, T., 2004. The influence of geological factors on indoor radon concentrations in Norway. *Sci. Total Environ.* 328, 41-53.

Swanson, R. W. (1961). *Geology and geochemistry of uranium in marine black shales: A review* (Professional Paper 356-C). Washington, DC: U.S. Geological Survey

Swanson, V. E., 1960, Oil yield and uranium content of black shales: U.S. Geol. Survey Prof. Paper 356-A, 44 p.

Szalay, A., 1954, The enrichment of uranium in some brown coals in Hungary: *Acad. Sci. Hungaricae, Acta Geol.*, v. 2, nos. 3-4, p. 299-310.

United States Geological Survey. The national geologic map database. 2019. [https://ngmdb.usgs.gov/ngmdb/ngmdb\\_home.html](https://ngmdb.usgs.gov/ngmdb/ngmdb_home.html). Accessed 13 July 2019.

UNSCEAR – United Nations Scientific Committee on the Effects of Atomic Radiation, 2000. Sources and Effects of Ionizing Radiation, Report to the General Assembly with Scientific Annexes. United Nations, New York. - Available on: [http://www.unscear.org/docs/publications/2000/UNSCEAR\\_2000\\_Report\\_Vol.I.pdf](http://www.unscear.org/docs/publications/2000/UNSCEAR_2000_Report_Vol.I.pdf)> (accessed: 03.01.2017)

van der Graaf, E.R., Koomans, R.L., Limburg, J., and de Vries, K., 2007, In situ radiometric mapping as a proxy of sediment contamination: Assessment of the underlying geochemical and -Physical Principles: Applied Radiation and Isotopes, v. 65, p. 619–633, doi: 10.1016/j.apradiso.2006.11.004.

[a] van der Veeke, S., Limburg, J., Koomans, R.L., Söderström, M., and van der Graaf, E.R., 2021, Optimizing gamma-ray spectrometers for UAV-borne surveys with Geophysical Applications: Journal of Environmental Radioactivity, v. 237, p. 1–14, doi: 10.1016/j.jenvrad.2021.106717.

[b] van der Veeke, S., Limburg, J., Koomans, R.L., Söderström, M., de Waal, S.N., and van der Graaf, E.R., 2021, Footprint and height corrections for UAV-borne gamma-ray spectrometry studies: Journal of Environmental Radioactivity, v. 231, p. 1–14, doi: 10.1016/j.jenvrad.2021.106545.

Van Wijngaarden, M., Venema, L.B., De Meijer, R.J., Zwolsman, J.J.G., Van Os, B., Gieske, J.M.J., 2002. Radiometric sand–mud characterization in the Rhine-Meuse estuary. Part A. Fingerprinting. *Geomorphology* 43, 87–101.

Vaupotič, J., Gregorič, A., Kobal, I., Zvab, P., Kozak, K., Mazur, J., Kochowska, E., and Grządziel, D.: Radon concentration in soil gas and radon exhalation rate at the Ravne Fault in NW Slovenia, *Nat. Hazards Earth Syst. Sci.*, 10, 895–899, doi:10.5194/nhess-10-895-2010, 2010.

Veeger, A. I., and Ruderman, N. C. (1998). Hydrogeologic controls on radon-222 in a buried valley-fractured bedrock aquifer system. *Ground Water* 36, 596-604.

Vienneau, D., de Hoogh, K., Hauri, D., Vicedo-Cabrera, A. M., Schindler, C., Huss, A., et al. (2017). Effects of radon and UV exposure on skin cancer mortality in Switzerland. *Environmental Health Perspectives*, 125, 067009. <https://doi.org/10.1289/EHP825>

VoPham, T., DuPré, N., Tamimi, R. M., James, P., Bertrand, K. A., Vieira, V., et al. (2017). Environmental radon exposure and breast cancer risk in the nurses' health study II. *Environmental Health*, 16, 97. <https://doi.org/10.1186/s12940-017-0305-6>

Weir, G. W., and Greene, R. C., 1965, Clays Ferry Formation (Ordovician) – A new map unit in south-central Kentucky: *U.S. Geol. Survey Bull.* 1224-B, p. B1-B18.

[a] What is background radiation? Is background radiation a risk to me and my family?, 2022, EPA, <https://www.epa.gov/radiation/what-background-radiation-background-radiation-risk-me-and-my-family> (accessed March 2023).

[b] What is radon gas? Is it dangerous?, 2022, EPA, <https://www.epa.gov/radiation/what-radon-gas-it-dangerous> (accessed February 2023).

## VITA

### EDUCATION

May 2021                                      Geological Sciences B.A. University of Kentucky

### PROFESIONAL EXPERIENCE

Graduate Researcher, Department of Earth and Environmental Sciences, University of Kentucky, Lexington, KY: June 2021 to August 2023

Research Assistant, Kentucky Geological Survey, University of Kentucky, Lexington, KY: June 2021 to May 2023

Paul Edwin Potter Internship, Kentucky Geological Survey, University of Kentucky, Lexington, KY: May 2022 to July 2022

Student – Employee, Kentucky Geological Survey, University of Kentucky, Lexington, KY: August 2019 to May 2021

### SCHOLASTIC AND PROFESSIONAL HONORS

2022                                      Kentucky Association of Mapping Professional Scholarship

2022                                      GSA EEG Division Graduate Poster Competition – 1<sup>st</sup> place

2021-2023                              Lyman T. Johnson Fellowship

2021                                      Steve and Cindie Sullivan Excellence Award

2020-2021                              Sigma Gamma Epsilon Inductee



2020

Pirtle Outstanding Senior Undergraduate Award

#### PROFESSIONAL PUBLICATIONS

Thomas, A., Andrews, W., Crawford, M., and Haneberg, W., 2022, Field tests of a UAV-compatible spectrometer to evaluate its suitability for detailed soil radon potential mapping: Geological Society of America Abstracts with Programs, v. 54, no. 5, <https://doi.org/10.1130/abs/2022AM-380324>.

Alexandria Briahnne Thomas